

*1145-CR
193071
97P*

Biophysical Characterization and Surface Radiation Balance

**Final Report for Period
September 15, 1991 - September 14, 1993**

NASA Grant NAG5-1762

by

**Elizabeth A. Walter-Shea, Blaine L. Blad, Mark A. Mesarch,
Cynthia J. Hays and Patrick J. Starks**

**Department of Agricultural Meteorology
Institute of Agriculture and natural Resources
University of Nebraska-Lincoln 68583-0728**

(NASA-CR-194659) BIOPHYSICAL
CHARACTERIZATION AND SURFACE
RADIATION BALANCE Final Report, 15
Sep. 1991 - 14 Sep. 1993 (Nebraska
Univ.) 97 p

N94-17762

Unclas

G3/45 0193071

Introduction

"The Kursk 1991 Experiment (KUREX-91) was conducted as one of a suite of international studies to develop capabilities to monitor global change" (Deering and Konzoderov, 1992). The studies were designed specifically to understand the earth's land-surface vegetation and atmospheric boundary layer interaction. An intensive field campaign was conducted at a site near Kursk, Russia during the month of July in 1991 by a team of international scientists to aid in the understanding of land-surface-atmosphere interactions in an agricultural/grassland setting.

We were one of several teams of scientists participating at KUREX-91 at the Streletskaya Steppe Reserve near Kursk, Russia. The main goals of our research were to:

1. characterize biophysical properties of the prairie vegetation
2. characterize radiation regime through measurements and from estimates derived from canopy bidirectional reflectance data.

Four objectives were defined to achieve these goals:

1. Determine dependence of leaf optical properties on leaf water potential of some dominant species in discrete wavebands in the visible, near-infrared and mid-infrared (spanning 0.4-2.3 μm range).
2. Characterize the effective leaf area index (LAI) and leaf angle distribution of prairie vegetation.
3. Characterize the radiation regime of the prairie vegetation through measures of the radiation balance components
4. Examine, develop and test methods for estimating albedo, APAR and LAI from canopy bidirectional reflectance data.

The following papers are the result of our research efforts. The papers have been submitted to Remote Sensing Reviews for publication.

REFERENCE:

Deering, D.W., and V. V. Kozoderov. 1992. KUREX-91: A USSR/US Study for global climate processes in steppe vegetation, Proc. International Geosc. and Remote Sens. Symp., May 26-29, 1992, Houston, Texas, pp. 1035-1038.

COMPARING BIOPHYSICAL PROPERTIES OF THE STRELETSKAYA STEPPE RESERVE AND THE KONZA PRAIRIE¹

M.A. Mesarch², E.A. Walter-Shea, B.L. Blad, C.J. Hays
Department of Agricultural Meteorology
University of Nebraska-Lincoln
Lincoln, Nebraska

E.M. Middleton
NASA Goddard Space Flight Center
Greenbelt, Maryland

Keywords: biophysical properties, canopy architecture, FIFE, KUREX, leaf optical properties.

ABSTRACT

Reflected radiation by a crop canopy can be influenced by changes in the biological processes and attributes of the canopy. The study was conducted to characterize the effective leaf area index (LAI) and leaf angle distribution of the Streletskaia Steppe Reserve of the Russian Republic and the Konza Prairie in Kansas and to determine dependence of leaf optical properties on leaf water potentials of some dominant species in discrete wavebands in the visible and near-infrared (NIR) (spanning 0.4–1.0 μm range). Biophysical properties were measured in July 1991 on the reserve for the Kursk Experiment (KUREX-91) and at the prairie during the summer of 1989 for the First ISLSCP Field Experiment (FIFE-89). Leaf area index, leaf angle distribution, mean tilt angle, canopy height, leaf optical properties, and leaf water potential were measured. Generally, the KUREX-91 steppe sites were characterized by high leaf area index and an uniform leaf angle distribution, while the FIFE-89 prairie sites were characterized by low leaf area index and an erectophile canopy. The magnitude of the leaf optical properties is variable between species; a significant difference between plant groups and between locations was detected for reflectance, but not generally for transmittance. Leaf optical properties are not related to leaf water potential (over the -0.5 to -3.5 MPa range) for dominant plant species observed at the KUREX-91 and FIFE-89 sites. Characterization of the biophysical properties during the FIFE-89 and KUREX-91 experiments provide information useful in understanding the differences in canopy bidirectional reflectance observed at the two grasslands.

INTRODUCTION

Reflected radiation by a crop canopy can be influenced by changes in the biological processes and attributes of the canopy. Optical properties of individual leaves depend upon many factors including water content (Thomas *et al.*, 1971; Bowman 1989), internal cellular structure (Gates *et al.*,

¹Published as Paper No. _____, J. Ser., Nebraska Agric. Res. Div. Received _____ 1993, Revised _____.

²Address correspondence to: M.A. Mesarch, Dept. of Agric. Meteorology, University of Nebraska, 107 L.W. Chase Hall, Lincoln, NE 68583-0728

1965; Gausman *et al.*, 1969; Gausman, 1974) and surface characteristics (Breece & Holmes, 1971; Grant, 1987). Leaf orientation along with illumination and view geometry create a intricate system of reflected and transmitted radiation so reflectance from a canopy can differ with canopy geometry (Jackson & Pinter, 1986). Reliable interpretation of remote sensing data, requires monitoring and measurement of biological processes and canopy attributes to understand radiant energy interaction and the resulting reflected signal. Biophysical properties were measured at the Streletskaaya Steppe Reserve of the Russian Republic in the former Soviet Union in July 1991 for the Kursk Experiment (KUREX-91). Similar properties were also measured at the Konza Prairie in Kansas, USA during the summer of 1989 for the First ISLSCP Field Experiment (FIFE-89) (Walter-Shea *et al.*, 1992).

The overall goal is to characterize and contrast the biophysical properties of selected sites at the Streletskaaya Steppe Reserve and the Konza Prairie during KUREX-91 and FIFE-89, respectively. Specific objectives were: 1) characterize the effective leaf area index (LAI) and leaf angle distribution of the grasslands; and 2) determine dependence of leaf optical properties on leaf water potentials of some dominant species in discrete wavebands in the visible and near-infrared (NIR) (spanning 0.4-1.0 μm range).

MATERIALS AND METHODS

Site Description

Biophysical properties of the KUREX-91 steppe were measured between 7 July 1991 and 26 July 1991 in plots located within or near the 50m x 50m canopy reflectance area (Deering & Kozoderov, this issue) at each of three sites (sites 12, 13 and 14.) Harvest practices varied between the sites. Site 12 was mown three out of every four years and was last mown two years before the experiment. Site 13 was mown the year before the experiment and also just prior to the experiment. Site 14 was absolutely reserved. Leaf area index, mean tilt angle, leaf angle distribution, canopy height, described in this paper and canopy temperature and fraction of instantaneous absorbed photosynthetically active radiation (fAPAR) described in Blad *et al.* (this issue) and Walter-Shea *et*

al. (this issue), respectively, were measured in five plots encircling the bidirectional canopy reflectance area (Figure 1). Each plot was 3m x 3m with the plot corners orientated in the cardinal directions. All measurements, except the LAI, for each of the plots were coordinated with the canopy reflectance measurements. Two plots of approximately 15m x 10m in size and separated by about 100m were used for measurements of leaf optical properties and leaf water potential (Ψ_L). These two plots were located to the east of the canopy reflectance area at site 12 and to the north at site 14; measurements of these properties were not made at site 13.

Biophysical properties of the FIFE-89 prairie were measured between 25 July 1989 and 12 August 1989 with a similar field design as at the steppe (Deering *et al.*, 1992 and Walter-Shea *et al.*, 1992) at two sites: site 906(2133-ECA) and site 911(4439-PAM). Leaf optical properties and Ψ_L were measured northeast of the canopy reflectance area at both sites.

Canopy Architecture

Leaf area index, mean tilt angle and leaf angle distribution were estimated with the LI-COR³ (P.O.Box 4425, Lincoln, NE, USA 68504) LAI-2000 Plant Canopy Analyzer at the steppe and the prairie. The instrument uses light penetration theory and the assumption of opaque leaves to infer these parameters (Welles & Norman, 1991). The mean tilt angle is the orientation of the canopy elements (elements including leaves, stems, etc.) from the horizontal. A 270 degree view cap was mounted on the instrument lens to restrict the instrument's field of view including the operator's silhouette. A black tarp was used to shade the canopy in the instrument's field of view to meet the diffuse light requirement for LAI estimations for the measurements on the steppe. Mean tilt angle and leaf angle distribution measurements do not require the canopy to be shaded. Measurements were replicated three times within each plot during each measurement period coordinated with the canopy reflectance measurements (at designated solar zenith angles) and a daily average and standard

³ The use of company names and brand names are necessary to report factually on available data; however, the University of Nebraska and NASA/GSFC neither guarantee nor warrant the standard of the product, and the use of the name by the University of Nebraska and NASA/GSFC implies no approval of the product to the exclusion of others that may also be suitable.

deviation were computed. LAI was measured at least once on the same day of canopy reflectance measurements. Leaf area index, mean tilt angle and leaf angle distribution of the prairie sites were estimated soon after dawn (solar zenith angles $> 75^\circ$) so shading of the canopy was not necessary. Five measurements per plot were made. Measurements on the prairie were made only once a day and only periodically throughout the experiment.

Heights of the tallest, shortest and medium foliage and inflorescence in each plot were measured on the steppe. Three replications of height yielded an average foliage and average inflorescence height for each site. Canopy heights were measured at all sites early in the experiment and again at site 12 after a heavy rainfall caused the vegetation to lodge. The tallest plant height and an average height per plot were measured on the prairie, once at each site from which an average height per site was calculated.

Leaf Optical Properties and Ψ_L

Leaf optical properties and Ψ_L were measured from randomly selected leaves of the dominant species. Dominant steppe grass species were from the genus *Bromus* L. (bromegrass) and *Calamagrostis* Adans. (reedgrass). Vegetative and reproductive growth stages were present. Dominant steppe forb species were *Salvia* L. (sage), *Veratrum* L. (false hellebore) and *Fragaria virginiana* Duchn. (strawberry). Typically, two leaves of each grass species and growth stage were measured at each plot on one site on each day of measurement. Forb species were measured only several times during the entire experiment. Dominant prairie grass species were *Andropogon gerardii* Vitman (big bluestem), *Panicum virgatum* L. (switchgrass), *Sorghastrum nutans* (L.) Nash (indiangrass) and *Sporobolus asper* (Michx.) Kunth (tall dropseed). A similar selection strategy used on the steppe was also used on the prairie.

Hemispherical reflectance and transmittance at near-normal incidence were measured with the Nebraska Multiband Leaf Radiometer (NMLR) (Mesarch *et al.*, 1991) and the Spectron Engineering (225 Yuma Court, Denver, CO, USA 80223) SE590 spectroradiometer attached to a LI-

COR LI-1800 Integrating sphere. The NMLR is a custom-built radiometer which provides optical coverage in seven wavebands similar to those of the LANDSAT Thematic Mapper. Pre- and post-calibration of the NMLR indicated that only the first four wavebands were functioning properly during 1991; the nominal wavelength limits of these bandwidths are approximately 450-520 (blue visible), 520-600 (green visible), 630-690 (red visible) and 760-900 nm (near-infrared). The mean bias error of transmittance factors determined from calibration was approximately 0.75% for wavebands 1-4 (the error is assumed to be of similar magnitude for reflectance.) The SE590 is a high spectral resolution radiometer which measures over the 400 to 1100 nm wavelength range (wavebands approximately every 3 nm and a bandwidth of 10-15 nm per waveband.) The mean bias error of transmittance factors determined from the SE590 calibration was approximately 0.5% across all the wavebands (the error is assumed to be of similar magnitude for reflectance.) Comparison of transmittance from neutral density filters measured with the NMLR and the SE590 (integrated over the half-bandwidth wavelengths of the NMLR wavebands) demonstrate that the NMLR and SE590 are comparable with mean bias errors of -0.15%, -1.08%, -0.71% and -0.76% for wavebands one through four, respectively. The standard light source for the LI-COR Integrating sphere illuminates a 1.14 cm diameter spot size on the leaf sample target. A standard light source was modified to produce a narrow light beam (3.5 mm x 11mm spot size), ideal for narrow leaf measurements. The modified light source was used with the SE590 on the steppe and the NMLR at both the steppe and prairie. Only a standard light source was used with the SE590 at the prairie. Two leaves were taped together to form the sample, so as to encompass the entire light beam from the standard light source. Table 1 contains the number of samples measured by species, instrument and experiment.

Leaf water potential was measured at both the steppe and prairie with a Scholander-type pressure chamber (Precision Machine Co., 2933 'N' St., Lincoln, NE, USA, 68504) on the same leaves as had been used for the leaf optical properties (Stewart & Nielson, 1990). Typically, two to four additional leaves from surrounding plants of the same species were also measured.

Leaf optical properties and Ψ_L were measured periodically on days of canopy reflectance measurements and also on other days independent of sky conditions.

Statistical Approach

SE590 data were integrated over the half-bandwidths wavelengths of the NMLR to combine datasets from both radiometers for manageable comparison of leaf optical properties. A pairwise comparison of the mean leaf optical properties by species, plant group and experiment was conducted using a Tukey HSD test, with a Tukey-Kramer adjustment for unequal sample sizes (SYSTAT, Inc., 1800 Sherman Ave., Evanston, IL USA 60201-3793.) Mean differences were considered significantly different below the 5% probability level and considered highly significant below the 1% probability level.

RESULTS and DISCUSSION

Canopy Architecture

The LAI of the KUREX-91 steppe site 13 was similar to the LAI at FIFE-89 prairie sites 906 and 911 while the LAI at steppe sites 12 and 14 was considerably larger (Figure 2). The large variations in LAI, especially at site 14, are undetermined. The mean and standard deviations of leaf angle distribution and mean tilt angle for the prairie sites were approximately the same. The average leaf angle distribution and mean tilt angle of KUREX-91 site 13 were significantly different between 7 July 1991 and 26 July 1991. However, measurements on both dates for KUREX-91 site 13 were not significantly different than measurements throughout the FIFE-89 experiment and represent an erectophile canopy (Figure 3). The leaf angle distribution and mean tilt angle for steppe sites 12 and 14 are not significantly different from each other and represent a uniformly distributed canopy. Leaf angle distribution and mean tilt angle were not significantly different after the canopy lodged at steppe site 12.

Canopy heights were considerably smaller at KUREX-91 site 13 than at sites 12 and 14 (Table 2). Site 13 was mown so inflorescences were not present. FIFE-89 canopy heights at sites 906 and 911 were larger than the canopy height at KUREX-91 site 13.

Leaf Optical Properties

Reflectance and transmittance averaged over all grass species and all forb species are typical of spectra of healthy green vegetation (Knippling, 1970) (Figure 4). Properties measured by the SE590 and NMLR were not significantly different for the KUREX-91 data, but significant differences were found between the two radiometers in both reflectances and transmittances of the NIR (1.5-1.9%) in the FIFE-89 data. Differences between the measurements of the FIFE-89 grass leaves may be caused by the difference in measuring techniques used with the radiometers (i.e., SE590 measurements were made with a larger beam of light on two leaves taped together.) Although the differences between instruments for the KUREX-91 forbs were not significant, the reported differences may be influenced most by the limited sampling with the two radiometers.

A pooled data set from measurements made by both radiometers was created since there was a lack of statistical significant difference between radiometer and spectroradiometer across all wavebands. Each species was compared to the other and the ranges of the mean differences between species is presented in Table 3. The variations between leaf reflectance of steppe grass species were highly significant for vegetative bromegrass and the reedgrass in blue visible and NIR regions. Steppe grass leaf reflectances were also highly significantly different from sage and false hellebore reflectances in the green and red visible regions while the grasses were highly significantly different from the strawberry in NIR. Transmittance differences were highly significant between the bromegrass and the reedgrass in the visible region and between the reedgrass and the false hellebore in the NIR region.

A similar test was conducted on the four prairie grass species. Reflectance differences were highly significant between switchgrass and indiagrass and between switchgrass and big bluestem for measurements in the NIR region. Switchgrass transmittances were highly significantly different from the other grass species across all wavelength regions.

Each dominant species at KUREX-91 and FIFE-89 were compared to each other to see if leaf optical properties differed between the two experimental sites (Table 3). Bromegrass (vegetative growth stage) reflectance was highly significantly different from most of the prairie grass species reflectances in the blue visible and the NIR regions. Differences between the steppe sage and false

hellebore leaf reflectances and the prairie grass leaf reflectances were highly significant in the visible region; strawberry reflectance was highly significantly different than all the prairie grass reflectances. Steppe brome grass transmittance was highly significantly different than prairie switchgrass transmittance in the green visible region. Steppe vegetative reedgrass transmittance was highly significantly different than prairie big bluestem, indiagrass and tall dropseed transmittances in the blue visible region. Steppe reedgrass transmittance was highly significantly different than prairie big bluestem, indiagrass and tall dropseed transmittance in the red-visible region. The steppe forb transmittance were not statistically different from the prairie grass transmittance, except between strawberry and switchgrass in the NIR region.

Optical properties were generalized, for measurements by both the radiometer and the spectroradiometer, into grass and forb plant groups (since within group differences were generally small) to show general differences among plant groups between the two experimental sites (Table 3). The differences at the various wavelength regions is illustrated well with the SE590 spectral data averaged over the appropriate species group (Figure 5). Steppe grass group reflectance was highly significantly different from forb group reflectance across all regions and from prairie grass group reflectance in the NIR region (Table 3). The steppe grass group transmittance was significantly different than the forb group transmittance. The prairie grass group transmittance was significantly different than the steppe grass group transmittance in the red-visible region and significantly different from the steppe forb group transmittance in the NIR region. Variation between individual grass and forb species was twice as large as variation between plant groups.

Leaf Water Potential

Leaf water potentials ranged from -0.5 to -3.5 MPa during the July measurement period at KUREX-91 (Figure 6). The ψ_L measured within hours soon after dawn (21 July 91) ranged from -0.5 to -2 MPa, while ψ_L measured afterwards ranged from approximately -1.0 to -3.5 MPa. The vegetative growth stage reedgrass plants recovered more than the reproductive growth stage reedgrass plants. Leaf water potentials measured in the afternoon (on two occasions) were slightly greater than those

measured in the mid-morning hours, however, precipitation had occurred in the previous 24 hours of these days. Leaf water potentials indicate the steppe vegetation was stressed early in the day which was slightly alleviated during the night or when some moisture was provided. Pre-dawn leaf water potentials of plants at FIFE-89 (-0.1 to -1.25 MPa) indicated that the FIFE-89 plants tended to recover over night from stress conditions of -1.0 to -3.0 MPa during the day (Figure 6).

Leaf Optical Property and Ψ_L Relationship

Leaf optical properties of the KUREX-91 steppe vegetation did not vary significantly with Ψ_L over the range of -0.5 to -3.5 MPa (Figure 7). Similar results were observed at FIFE-89 (Walter-Shea *et al.*, 1992). Thus differences in leaf optical properties between species and plant groups cannot be explained by Ψ_L over the range observed.

CONCLUSIONS

The biophysical property measurements collected during KUREX-91 and FIFE-89 provide information useful in understanding canopy bidirectional reflectances observed at the Streletskaya Steppe and the Konza Prairie. Generally, the KUREX-91 steppe sites were characterized by high LAIs and an uniform leaf angle distribution, while the FIFE-89 prairie sites were characterized by low LAIs and an erectophile canopy. The magnitude of the leaf optical properties is variable between species; significant differences between plant groups and between locations were detected for leaf reflectance, but not generally for leaf transmittance. Leaf optical properties appear not to be related to leaf water potential over the observed range of -0.5 to -3.5 MPa for dominant plant species observed at the KUREX-91 and FIFE-89 sites.

ACKNOWLEDGEMENTS

The authors would like to thank the Russian and United States scientists and students who helped collect the data during the two experiments. This work was supported by the National Aeronautics and Space Administration under Grants No. NAG5-1762 and NAG5-894. (in-house reviewers)

~~XXXXXXXXXX~~ ~~XXXXXXXXXX~~

XXXXXXXXXX

REFERENCES

- Blad, B.L., Walter-Shea, E.A., Mesarch, M.A., Hays, C.J., Deering D.W. and Eck, T.F. (This issue)
NEW TITLE Estimating reflected and emitted components of the radiation balance using
remotely sensed spectral data from KUREX-91
- Bowman, W.D. 1989. The relationship between leaf water status, gas exchange and spectral
reflectance in cotton leaves. *Remote Sens. Environ.* 30:249-255.
- Breece, H.T., III and Holmes, R.A. 1971. Bidirectional scattering characteristics of healthy green
soybean and corn leaves in vivo. *Appl. Opt.* 10:119-127.
- Deering, D.W. and Kozoderov, V.V. (this issue) NEW TITLE KUREX-91: A U.S.S.R./U.S. study for
global climate processes in steppe vegetation
- Deering, D.W., Middleton, E.A., Irons, J.R., Blad, B.L., Walter-Shea, E.A., Hays, C.J. and Walthall,
C. 1992. Prairie grassland bidirectional reflectances measured by different instruments at the
FIFE site. *J. Geophys. Res.* 97(D17):18887-18903.
- Gates, D.M., Keegan, H.J., Schleter, J.C. and Weidner, V.R. 1965. Spectral properties of plants. *Appl.*
Opt. 4(1):11-20.
- Gausman, H.W. 1974. Leaf reflectance on near-infrared. *Photo. Engin.* 40(2):183-191.
- Gausman, H.W., Allen, W.A., Myers, V.I. and Cardenas, R. 1969. Reflectance and internal structure
of cotton leaves, *Gossypium hirsutum* L. *Agron. J.* 61:374-376.

PRECEDING PAGE BLANK NOT FILMED

- Grant, L. 1987. Diffuse and specular characteristics of leaf reflectance. *Remote Sens. Environ.* 22:309-322.
- Jackson, R.D. and Pinter, Jr., P.J. 1986. Spectral response of architecturally different wheat canopies *Remote Sens. Environ.* 20:43-56.
- Knipling, E.B. 1970. Physical and physiological basis for the reflectance of visible and near-infrared radiation from vegetation. *Remote Sens. Environ.* 1:155-159.
- Mesarch, M.A., Walter-Shea, E.A., Robinson, B.F., Norman J.M. and Hays, C.J. 1991. Performance evaluation and operation of a field-portable radiometer for individual leaf optical measurements. University of Neb.-Lincoln. AgMet Progress Report 91-2.
- Stewart, B.A. and Nielson, D.R. (ed.) 1990. "Irrigation of agricultural crops." ASA, CSSA, SSSA. pp. 251-257.
- Thomas, J.R., Namkem, L.N., Oerther, G.F. and Brown, R.G. 1971. Estimating leaf water content by reflectance measurements. *Agron. J.* 63:845-847.
- Walter-Shea, E.A., Blad, B.L., Hays, C.J., Mesarch, M.A., Deering, D.W. and Middleton, E.A. 1992. Biophysical properties affecting vegetative canopy reflected and absorbed photosynthetically active radiation at the FIFE site. *J. Geophys. Res.* 97(D17):18925-18934.
- Walter-Shea, E.A., Blad, B.L., Mesarch, M.A., Hays, C.J. and Deering, D.W. (this issue) **NEW TITLE** Absorbed photosynthetically active radiation on steppe vegetation and sun-view-target geometry effects on APAR estimates.

Welles, J.M. and Norman, J.M. 1991. Instrument for indirect measurement of canopy architecture.
Agron. J. 83(5):818-825.

LIST of FIGURES

Figure 1 - General site layout for KUREX-91 indicating the relative locations of various measurement plots to the bidirectional canopy reflectance measurement area. Numbers 1 through 5 represent the plots for measurements of leaf area index, mean tilt angle, leaf angle distribution and canopy height measurements. Numbers 6 and 7 represent the plots of leaf optical properties and leaf water potential measurements.

Figure 2 - Estimated leaf area index (using LI-COR LAI-2000 Plant Canopy Analyzer) for selected KUREX-91 and FIFE-89 sites. Lines represent trends in the data at each site.

Figure 3 - Leaf angle distributions and mean tilt angle (MTA) for selected KUREX-91 and FIFE-89 sites. KUREX-91 site 13¹ leaf angle distributions were measured 7 July 91. KUREX-91 site 13² leaf angle distributions were measured 26 July 91.

Figure 4 - Average leaf reflectance and transmittance measured with Spectron Engineering SE590 Spectroradiometer (Solid lines) and Nebraska Multiband Leaf Radiometer (NMLR)(points) attached to a LI-COR Integrating sphere. Dashed lines and error bars represent one standard deviation from the mean. a) KUREX-91 grasses, b) KUREX-91 forbs and c) FIFE-89 grasses. No error bars are present for NMLR KUREX-91 forb leaf optical properties since only two samples were measured.

Figure 5 - Average leaf optical properties measured with the SE590 and integrating sphere. a) Comparison of KUREX-91 grass species group and forb species group b) Comparison of KUREX-91 and FIFE-89 grass species group.

Figure 6 - Measurement of leaf water potential (ψ_L) over time by species. a) KUREX-91 and b) FIFE-89.

Figure 7 - Leaf optical properties of dominant species at KUREX-91 as a function of Ψ_L . Leaf optical properties were measured with SE590 (integrated over the NMLR bandwidth limits) and NMLR, attached to an integrating sphere. Open symbols represent leaf optical properties for waveband 3 (630-690 nm) and solid symbols represent waveband 4 (760-900 nm). **a)** Reflectance and **b)** Transmittance.

Table 1 - The number of samples measured for leaf optical properties for each dominant species at KUREX-91 and FIFE-89 using the Nebraska Multiband Leaf Radiometer (NMLR) and a Spectron SE590 attached to a LI-COR integrating sphere.

EXPERIMENT	SPECIES	RADIOMETER		TOTAL
		NMLR	SE590	
KUREX-91	Bromegrass - Vegetative	16	10	26
	Bromegrass - Reproductive	14	8	22
	Reedgrass - Vegetative	28	12	40
	Reedgrass - Reproductive	14	4	18
	Sage	2	3	5
	False Hellebore	2	3	5
	Strawberry	2	3	5
FIFE-89	Big bluestem	34	10	44
	Indiangrass	39	11	50
	Switchgrass	28	6	34
	Tall dropseed	7	0	7

Table 2 - Mean and standard deviation of canopy height for the selected sites of KUREX-91 and FIFE-89. Sample size was 45, 15 and 5 for KUREX-91 foliage, KUREX-91 inflorescence and FIFE-89 foliage, respectively.

Location	Site	Date	Height (cm)	
			Foliage	Inflorescence
KUREX-91	12	July 10	52.8 ±21.0	133.2 ±6.7
		July 25	47.8 ±17.4	104.4 ±8.8
	13	July 10	14.8 ±6.8	N/A
	14	July 15	70.6 ±20.9	112.0 ±12.4
FIFE-89	906	August 7	29.0 ±8.7	N/A
	911	August 8	20.0 ±1.4	N/A

Table 3 - Range of mean differences from TUKEY HSD test of leaf optical properties for individual plant species and between plant group comparisons. Significant mean differences are below the 5% probability level. Individual refers to data pooled together between radiometers for each species. Group refers to data pooled between radiometers and plant group (i.e., grass or forb).

Data Comparisons	Reflectance (%)		Transmittance (%)	
	Non-significant	Significant	Non-significant	Significant
Individual: KUREX-91 grass	0.2 - 2.7	2.5 - 3.7	0.3 - 3.0	2.0 - 4.4
Individual: KUREX-91 forb	0.8 - 4.8	N/A	0.2 - 3.6	N/A
Individual: KUREX-91 grass and forb	0.4 - 4.3	3.2 - 9.3	0.4 - 3.3	5.6 - 5.9
Individual: FIFE-89 grass	0.1 - 0.9	1.7 - 2.1	0.3 - 3.0	1.1 - 3.7
Individual: KUREX-91 grass and FIFE-89 grass	0.0 - 2.5	1.9 - 5.1	0.0 - 3.2	1.4 - 3.4
Individual: KUREX-91 forb and FIFE-89 grass	0.1 - 4.6	2.7 - 7.8	0.1 - 4.1	6.1
Group: KUREX-91 grass and forb	N/A	3.0 - 4.9	0.0 - 0.1	2.6
Group: KUREX-91 grass and FIFE-89 grass	0.2 - 0.7	1.3	0.3 - 0.6	0.8
Group: KUREX-91 forb and FIFE-89 grass	N/A	2.7 - 5.5	0.6 - 1.0	2.3

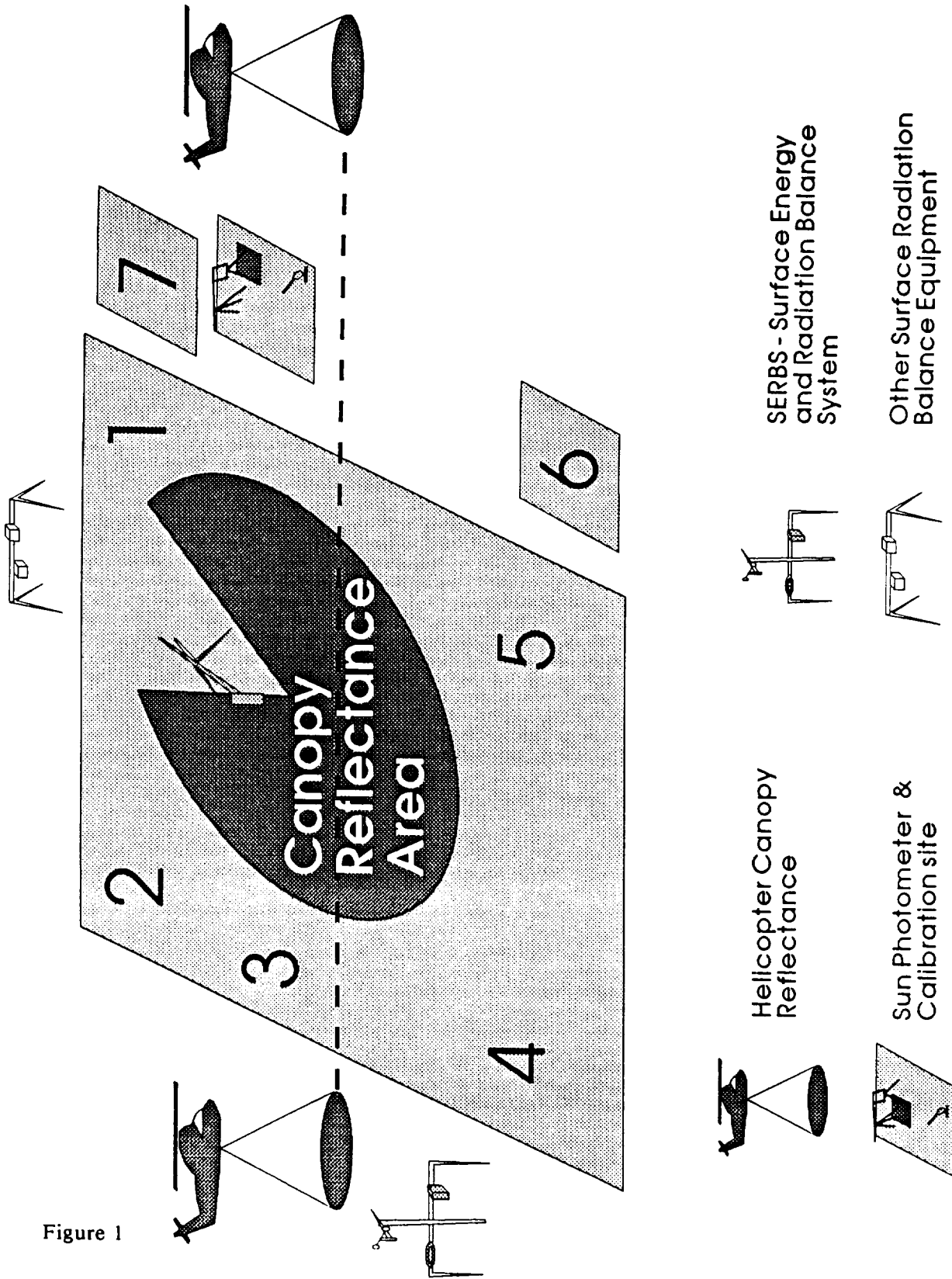
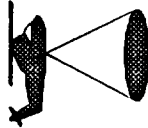
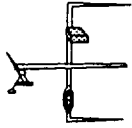
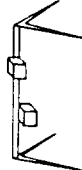
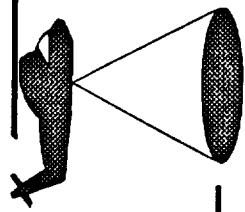
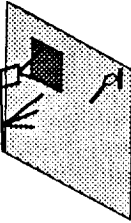
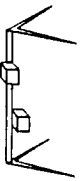


Figure 1

- 

 - 

 - 

 - 
- Helicopter Canopy Reflectance
 Sun Photometer & Calibration site
 SERBS - Surface Energy and Radiation Balance System
 Other Surface Radiation Balance Equipment

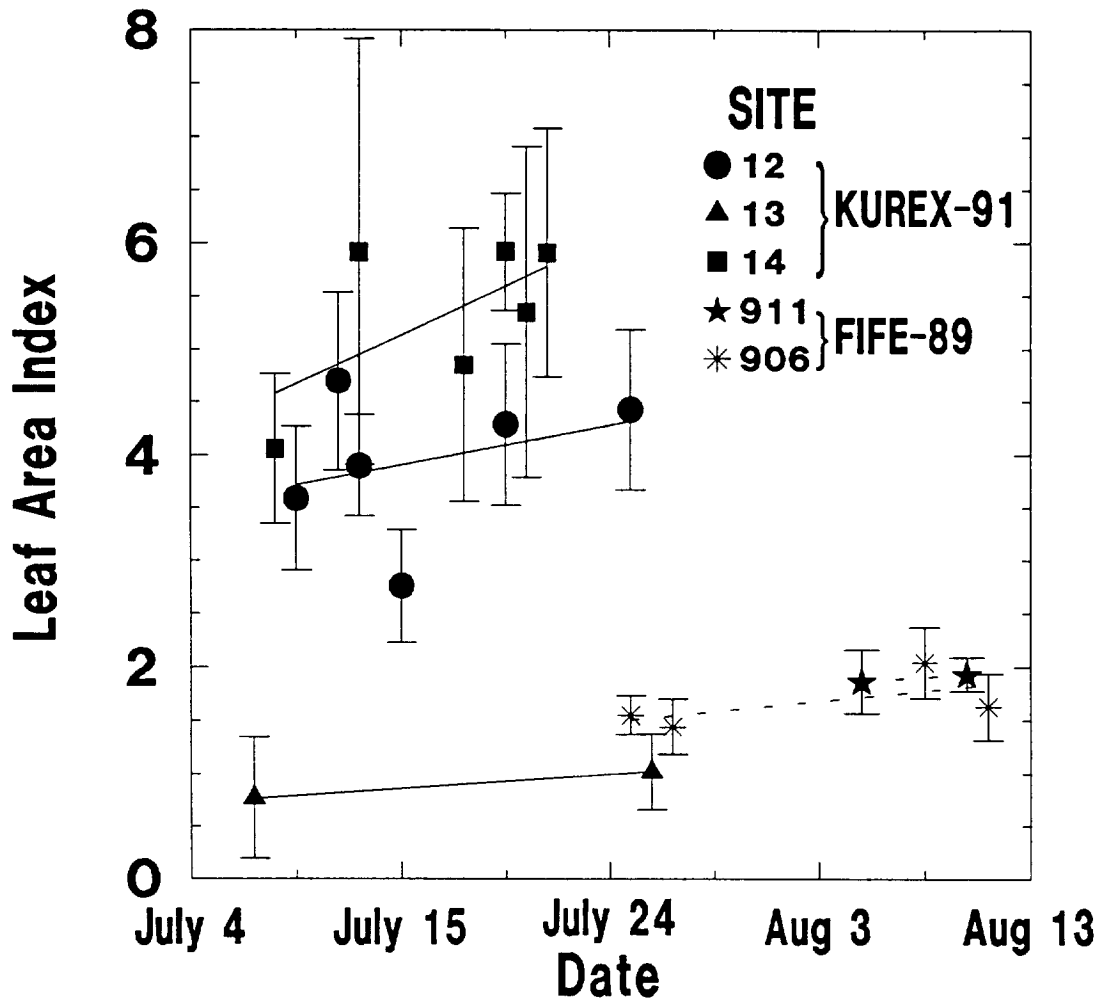


Figure 2

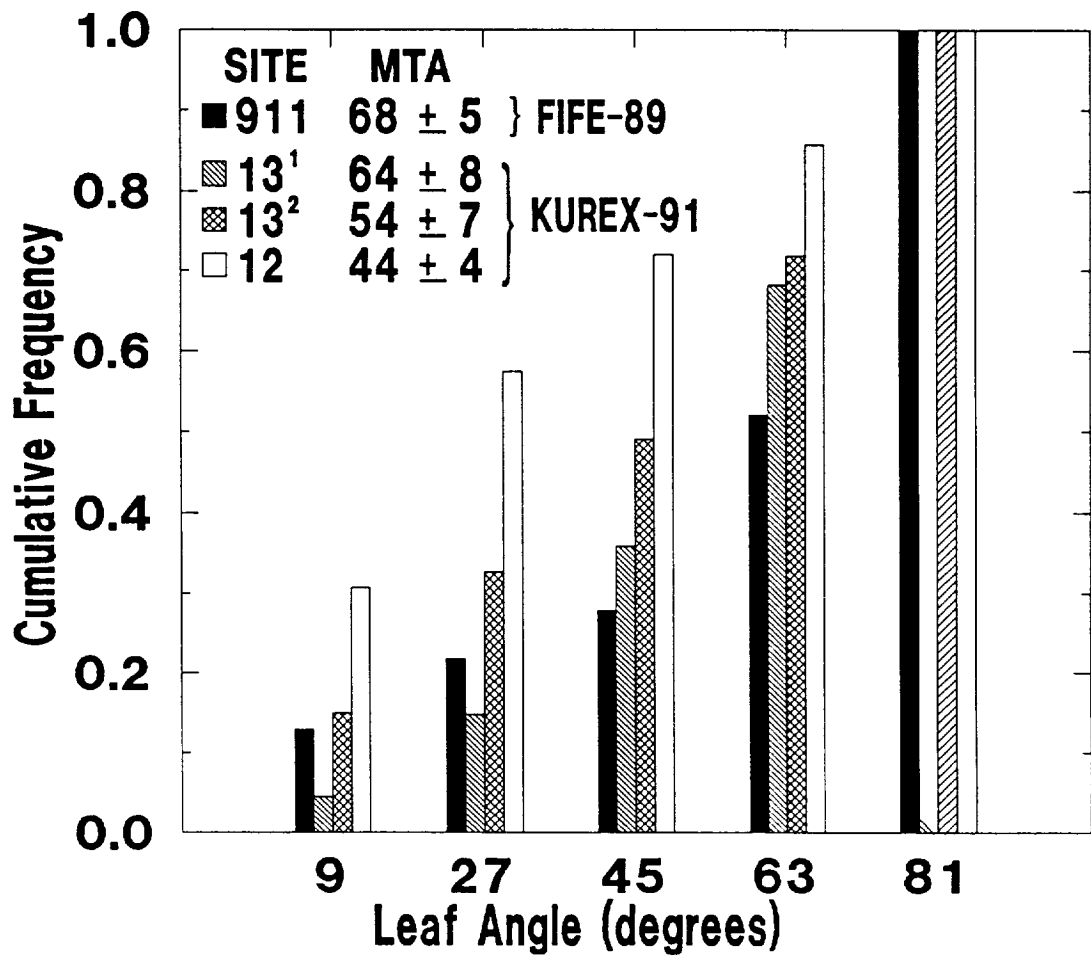
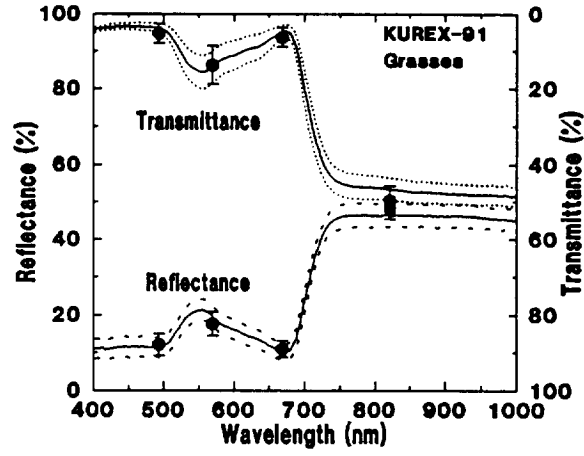
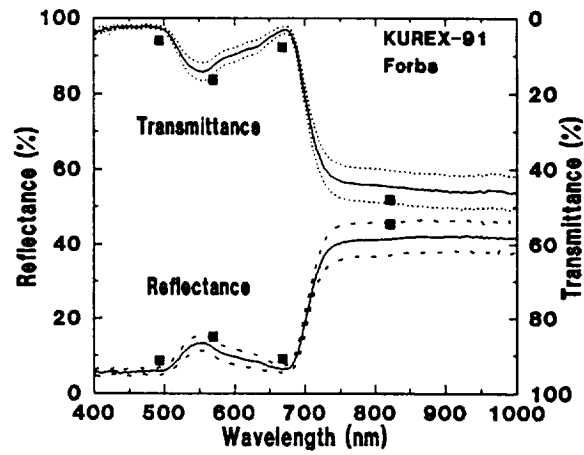


Figure 3

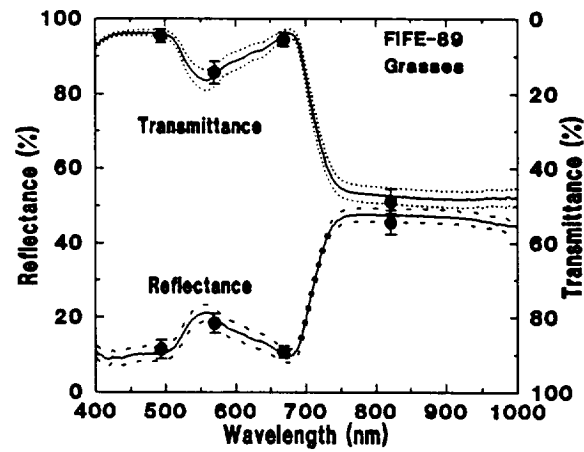
a)



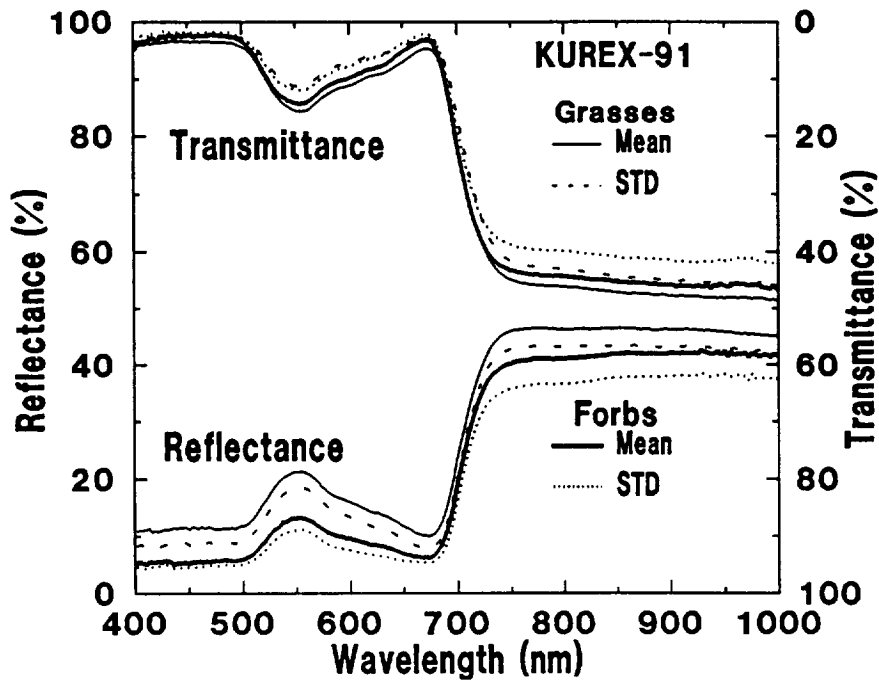
b)



c)



a)



b)

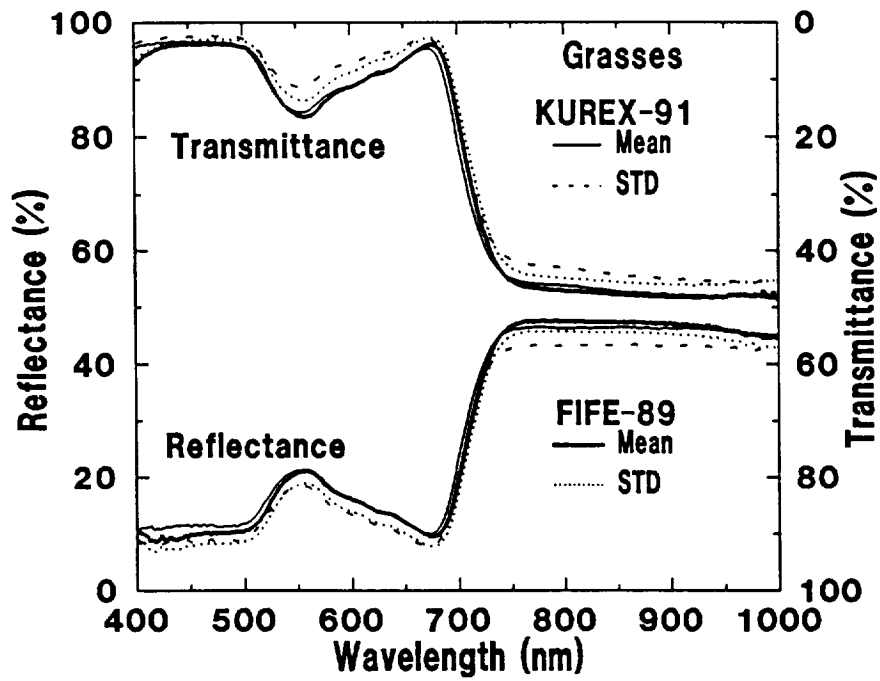
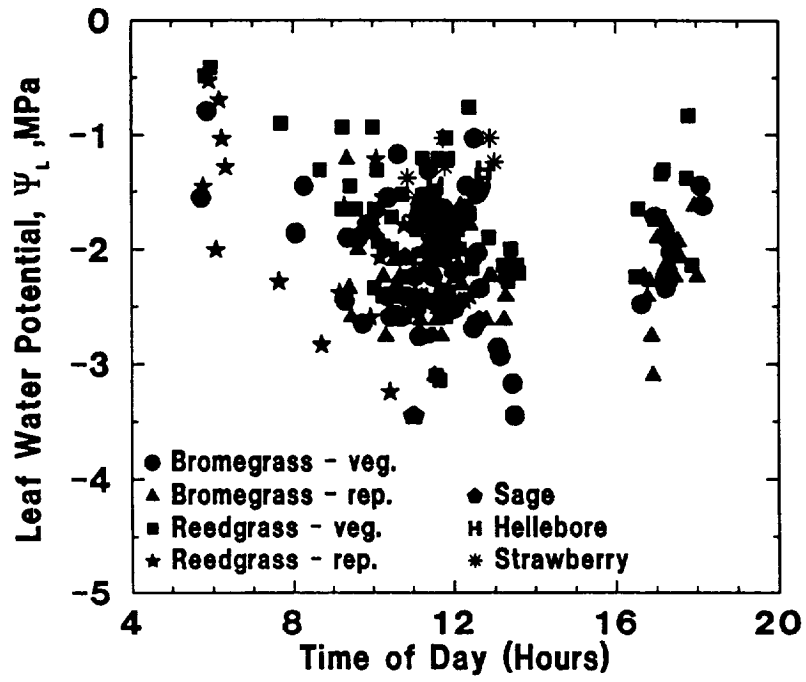


Figure 5

a)



b)

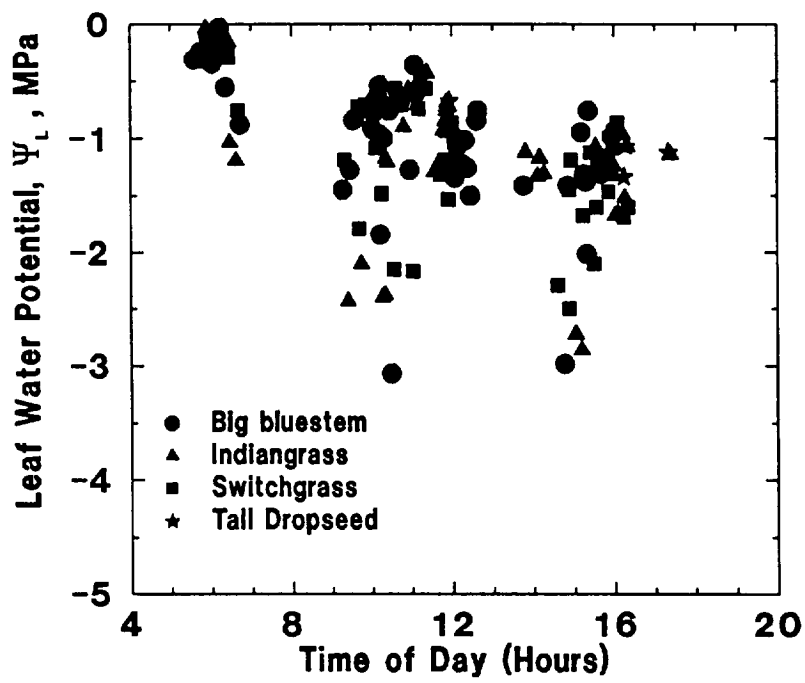
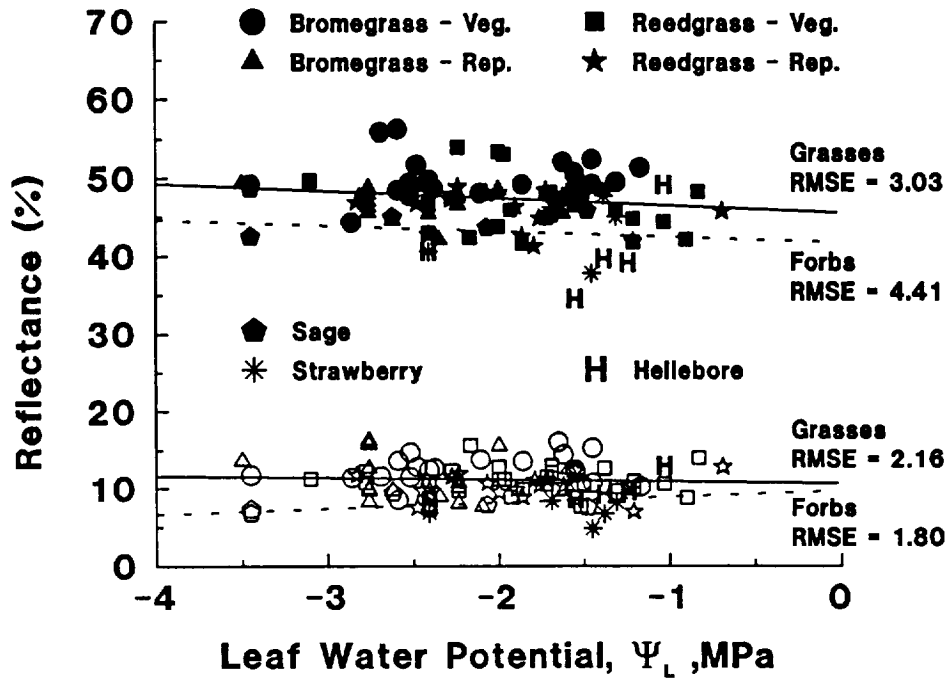


Figure 6

a)



b)

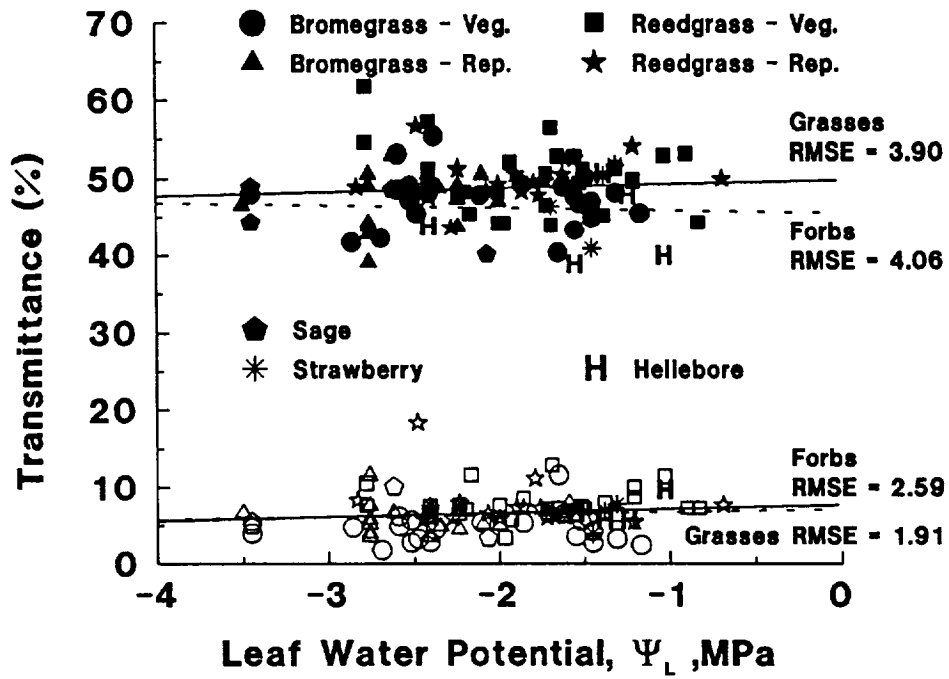


Figure 7

**ABSORBED PHOTOSYNTHETICALLY ACTIVE RADIATION AND
SUN-VIEW GEOMETRY EFFECTS ON REMOTE SENSING RELATIONSHIPS¹**

E.A. Walter-Shea*, B.L. Blad, M.A. Mesarch and C.J. Hays
Dept. of Agricultural Meteorology
University of Nebraska, Lincoln, NE

D.W. Deering and T.F. Eck
NASA/Goddard Space Flight Center
Greenbelt, MD

ABSTRACT

Photosynthetically active radiation (PAR) absorbed by vegetation is an essential parameter in understanding vegetative photosynthetic capacity and surface conductance used in regional and global carbon cycle studies. This study was conducted to contrast absorbed photosynthetically active radiation at the FIFE-89 Konza prairie site to that of the KUREX-91 steppe grassland site and to investigate variations in relationships between absorbed PAR and spectral vegetation indices derived from bidirectional reflectance factors. Incoming, reflected and transmitted PAR were measured from which fractions of reflected, transmitted and absorbed PAR were computed at selected FIFE prairie and KUREX steppe sites. Fractions of direct and diffuse PAR transmitted through a canopy were estimated as a means of understanding results. Fractions of absorbed PAR were much lower at the FIFE sites (ranging from 0.35 to 0.65) than those at KUREX (ranging from 0.75 to 0.95) and can be explained by differences between leaf area index, leaf angle distribution, and direct and diffuse sky conditions. Scattering of PAR may be

* Address correspondence to Dr. E.A. Walter-Shea, Dept. of Agric. Meteorology, Univ. of Nebraska, Lincoln, NE 68583-0728

¹Published as Paper No. _____, J. Ser., Nebraska Agric. Res. Div.

Received _____ 1993, revised _____.

an important parameter in canopy light penetration particularly at large LAI and large solar zenith angles. The magnitude of spectral vegetation indices computed and plotted as a function of the fraction absorbed did not differ considerably even though LAI and the fraction of absorbed PAR did. Adjusting for background improved the distinction between spectral vegetation indices at the two experimental sites. Relationships between fraction of absorbed PAR and spectral vegetation indices derived from bidirectional reflectance factors were not consistent over illumination and view angles.

Keywords: diffuse and direct PAR fractions, reflected and transmitted fractions of PAR, bidirectional reflectance factor, spectral vegetation index

INTRODUCTION

Photosynthetically active radiation (PAR) absorbed by vegetation is an essential parameter in understanding vegetative photosynthetic capacity and surface conductance values which are useful for regional and global carbon cycle studies. The amount of radiant energy attenuated in a canopy is a function of leaf optical properties, canopy architecture (i.e., leaf area index, leaf angle distribution and gap fraction) and the direct and diffuse PAR fractions. The partitioning of PAR into direct and diffuse components is dependent on atmospheric conditions and solar illumination angle. Thus, PAR fractions intercepted (fIPAR) and absorbed (fAPAR) by vegetation are functions of canopy architecture (Richardson & Wiegand, 1989), solar zenith angle (Pinter, 1993; Walter-Shea *et al.*, 1993a) and atmospheric conditions (Hipps *et al.*, 1983). Diurnal variation in fAPAR associated with canopy architecture could significantly affect estimates of fAPAR (Richardson & Wiegand, 1989). Remote sensing can provide data from which $fIPAR(\theta_s)$ and $fAPAR(\theta_s)$ potentially can be estimated using ratios of reflected visible and

near-infrared (NIR) radiant energy known as spectral vegetation indices (SVIs) (Asrar *et al.*, 1984). Two common SVIs are the simple ratio ($SR = NIR/red$) and the normalized difference vegetation index ($NDVI = [(NIR-red)/(NIR+red)]$). Huete (1988) proposed a soil adjusted vegetation index ($SAVI = [(NIR-red)/(NIR+red+0.5)]*(1.5)$) which in theory should remove the soil contribution to NDVI.

Recent emphasis in estimating global vegetative cover and productivity has led to the use of NOAA-AVHRR (Advance Very High Resolution Radiometer) data measured at view zenith angles 56° either side of nadir to analyze biophysical parameters on regional and global scales. Spectral vegetation indices must retain sensitivity to surface characteristics while being relatively independent of sun and view angles if they are to provide reliable remotely-sensed estimates of surface conditions (Pinter *et al.*, 1987). However, SVIs have been shown to vary as a function of illumination and viewing geometry (Wardley, 1984; Shibayama *et al.*, 1987; Deering & Middleton, 1990; Middleton, 1991). Nadir-derived SVIs in alfalfa changed with solar zenith angle in a similar manner as $fAPAR(\theta_s)$ (Pinter, 1993). Thus, relationships between nadir-derived SVIs and $fAPAR(\theta_s)$ might hold over a range of solar zenith angles (Bartlett *et al.*, 1990; Pinter, 1993). However, off-nadir-derived NDVI departs from the apparent nadir-derived NDVI linear relationship with $fAPAR(\theta_s)$ (Asrar *et al.*, 1992; Walter-Shea *et al.*, 1993a). Even when relationships kept similar form, relationships between off-nadir derived SVIs and $fAPAR(\theta_s)$ were solar and view zenith angle dependent (Walter-Shea *et al.*, 1993a) with the simple ratio apparently the most sensitive to sun-view geometry. Sellers (1985) demonstrated through the use of a simple radiative transfer model that SVI dependence on solar zenith angle was a function of canopy architecture and may diminish with large LAI. However, NDVI became less

sensitive with sun-view geometry with increasing LAI in alfalfa while SR became increasingly dependent with sun-view geometry with increasing LAI (Walter-Shea *et al.*, 1993a).

The objectives of this paper are to 1) characterize and contrast instantaneous fractions of absorbed PAR [$fAPAR(\theta_s)$] in a moderate-cover prairie grassland (FIFE-89 sites) to that in a high-cover steppe grassland (KUREX-91 sites) and 2) investigate variations in the relationships between $fAPAR(\theta_s)$ and SVIs derived from BRFs.

MATERIALS AND METHODS

Incoming ($K_{\downarrow par}(\theta_s)$), reflected ($K_{\uparrow par}(\theta_s)$) and transmitted ($K_{\downarrow tpar}(\theta_s)$) PAR received on a one meter in length horizontal surface were measured with a LI-191SA Line Quantum Sensor² (LI-COR, Inc., Lincoln, NE 68504) above and within the prairie and steppe vegetation. PAR components were measured at five representative plots at FIFE-89 sites 906 and 911 and KUREX-91 sites 12 and 14. Measurements were coordinated with bidirectional canopy reflectance measurements. Fractions of reflected, transmitted, intercepted and absorbed PAR as functions of solar zenith angle [$fRPAR(\theta_s)$, $fTPAR(\theta_s)$, $fIPAR(\theta_s)$ and $fAPAR(\theta_s)$, respectively] were calculated from these measurements.

Fractions of reflected and transmitted PAR are simply the ratios of reflected and transmitted PAR to total incoming PAR, *i.e.*, $K_{\uparrow par}(\theta_s)/K_{\downarrow par}(\theta_s)$ and $K_{\downarrow tpar}(\theta_s)/K_{\downarrow par}(\theta_s)$, respectively. Instantaneous fractions of intercepted and absorbed PAR were calculated as:

²The use of company names and brand names are necessary to report factually on available data; however, the University of Nebraska and NASA neither guarantee nor warrant the standard of the product, and the use of the name by the University of Nebraska and NASA implies no approval of the product to the exclusion of others that may also be suitable.

$$fIPAR(\theta_s) = 1 - fTPAR(\theta_s) \quad (1)$$

$$fAPAR(\theta_s) = fIPAR(\theta_s) * (1 - fRPAR(\theta_s)) \quad (2)$$

In addition, a LI-190S Quantum Sensor (LI-COR Inc., Lincoln, NE 68504) was mounted on an A-frame for point measurements of incoming PAR and two LI-190S sensors were mounted within the canopy at the soil surface for measurements of transmitted PAR at KUREX site 14 (Fritschen, this issue). These measurements yielded near-continuous measurements of incoming and transmitted PAR from which $fTPAR(\theta_s)$ and $fIPAR(\theta_s)$ were calculated.

The fractions of PAR transmitted through the canopy which are direct [$fTPAR_{beam}(\theta_s)$] and diffuse [$fTPAR_{diffuse}(\theta_s)$] components were estimated following a procedure similar to that given by Fuchs *et al.* (1984).

Diffuse sky PAR penetration into a canopy of non-scattering leaves, $d(\theta_s)$, was computed as:

$$d(\theta_s) = (1/\pi) \int \int f(\theta, \phi, \theta_s) r(\theta) \sin\theta \cos\theta \, d\theta \, d\phi \quad (3)$$

where θ is the zenith angle of an unscattered ray of sky diffuse PAR between 0 and $\pi/2$, ϕ is the azimuth angle of the diffuse ray between 0 and 2π , $f(\theta, \phi)$ is the relative hemispherical radiance distribution of clear sky (Steven, 1977) and $r(\theta)$ is the penetration of a ray given as

$$r(\theta) = \exp(-GL/\cos\theta) \quad (4)$$

where G is the canopy extinction coefficient, L is the leaf area index and $\cos\theta$ corrects for path length of the ray into the canopy at angle θ .

Scattered PAR within a canopy is small since most of the radiation is absorbed by leaves, so that the contribution of scattered PAR to total PAR penetration through a canopy can be considered negligible. Thus, the sum of the estimates of the sky direct and diffuse PAR fractions penetrating a non-scattering vegetative canopy is assumed to be equivalent to the measured transmitted fraction, $fTPAR(\theta_s)$, so that

$$fTPAR(\theta_s) = q(\theta_s)r(\theta_s) + (1-q(\theta_s))d(\theta_s) \quad (5)$$

$q(\theta_s)$ is the ratio of direct PAR to total PAR above the canopy at θ_s . Direct and total PAR were measured at FIFE-89 whereas only total PAR was measured at KUREX-91. Thus, sky direct and diffuse PAR components for the KUREX sites were estimated using the 5S atmospheric radiative transfer model using average input parameters from Halthore *et al.* (this issue) for July 14 and 20, 1991. Estimated values of $fTPAR(\theta_s)$ are compared to measured values to determine the validity of the equations from which the canopy diffuse and direct penetrated PAR components are estimated.

Canopy radiances at FIFE-89 site 911 were measured with a Barnes model 12-1000 modular multiband radiometer (MMR). The PARABOLA (Deering & Leone, 1986) was used to measure canopy radiances at the KUREX-91 sites.

The MMR measures reflected shortwave radiation in seven wavebands: 0.45-0.52 μm , 0.52-0.60 μm , 0.63-0.69 μm , 0.76-0.90 μm , 1.15-1.30 μm , 1.55-1.75 μm , and 2.08-2.35 μm .

The instrument was set with a 15° instantaneous field of view and was mounted on a portable mast that maintained a distance of 3.1 m from the soil surface. Reflected radiation was measured from seven view zenith angles in the solar principal plane: nadir and 20, 35 and 50° to either side of nadir.

The PARABOLA was mounted on the end of a 6m boom supported on a large tripod. The PARABOLA measures reflected and incident radiation in three wave bands: 0.65-0.67, 0.81-0.84 and 1.62-1.69 μm . The scanning head turns on two axes, which enables the acquisition of radiance data for almost the complete (4π) sphere in 15° instantaneous field of view.

Canopy reflected data were converted to units of spectral radiance ($\text{W m}^{-2} \text{sr}^{-1} \mu\text{m}^{-1}$) according to the technique of Markham *et al.* (1988). Nadir-viewed radiances measured over the reference panels were corrected for non-Lambertian properties following the techniques of Jackson *et al.* (1987) and Walter-Shea *et al.* (1993b) to yield estimates of irradiance. A 1.2 x 1.2 m moded sintered polytetrafluorethylene-based (Spectralon) panel (Labsphere Inc., North Sutton, NH) and a painted barium sulfate reference panel were calibrated for use at FIFE-89 and KUREX-91, respectively. Canopy spectral measurements were subsequently expressed as bidirectional reflectance factors (BRFs) which correct for irradiance differences and facilitates comparison within and among dates (Bauer *et al.*, 1981). The BRF was calculated as the ratio of the radiance measurements over the canopy to the irradiance estimated from a time-based linear interpolation (to estimate irradiance at the time of individual target measurements) (Robinson & Biehl, 1979).

The Normalized Difference Vegetation Index (NDVI), Simple Ratio (SR) and Soil Adjusted Vegetation Index (SAVI) were computed using BRFs collected from the multiband radiometers over vegetation representative of the vegetation from which $fIPAR(\theta_s)$ and $fAPAR(\theta_s)$ were measured (Walter-Shea *et al.*, 1992; Eck & Deering, this issue).

RESULTS AND DISCUSSION

Instantaneous fractions of absorbed PAR ($fAPAR(\theta_s)$) decreased with increasing solar zenith angles at high LAI KUREX-91 site 14 over solar zenith angles of 37 to 72° and ranged in value from 0.75 to 0.95 (Figure 1). In contrast, data collected at the First ISLSCP Field Experiment in 1989 (FIFE-89) and KUREX-91 site 12 indicated $fAPAR(\theta_s)$ values increased or remained constant as solar zenith angle increased over a range of 20-50° (see Walter-Shea *et al.*, 1992). Also, lower LAI, especially at FIFE-89 sites, yielded considerably smaller $fAPAR(\theta_s)$ than those at KUREX-91. Instantaneous fractions of reflected PAR [$fRPAR(\theta_s)$] were small at all sites and tended to increase or remain constant as solar zenith angle increased at all sites regardless of LAI (Figure 2). Diurnal variations in transmittance were strong in canopies of low LAI. Instantaneous fractions of transmitted PAR [$fTPAR(\theta_s)$] at KUREX-91 site 14 increased as solar zenith angle increased but decreased at all other sites (note: range of solar zenith angle was not consistent at all sites). Point quantum sensors indicated that $fTPAR$ continued to increase beyond those measured with the line quantum sensor as solar zenith angle increased. (Note: continuous measurements of $fTPAR(\theta_s)$ agree well with the discrete measurements from the line quantum sensor with a mean relative error of -1.8%). As a result $fAPAR(\theta_s)$ at site 14 decreased with solar zenith angle while at all other sites mean $fAPAR(\theta_s)$ generally increased as solar zenith angle increased over the range of measurements (Fig. 1). Contrasts in $fAPAR$

diurnal variation have been reported elsewhere and attributed to leaf display and row structure (Richardson & Wiegand, 1989).

A simple canopy radiative transfer model describing transmitted sky direct and diffuse PAR fractions penetrating a canopy was used to investigate the effect of canopy architecture and sky condition on $fTPAR(\theta_s)$. Transmitted PAR fractions were estimated following the procedures defined in Eqs. (3-5) using values of G and LAI representative of the selected FIFE-89 and KUREX-91 sites (see Mesarch *et al.*, this issue). A G value equal to 0.5 (representing a canopy with a spherical leaf angle distribution) and LAIs equal to 3.9 and 5.6 were used to represent KUREX-91 sites 12 and 14, respectively. A G value equal to $2(\sin\theta_s)/\pi$ (representing a canopy with a vertical leaf angle distribution) and LAIs of 1.5 and 1.9 were used to represent FIFE-89 sites 911 and 906, respectively. Estimated $fTPAR(\theta_s)$ agreed within 15% MRE for FIFE-89 sites and KUREX-91 site 12 (with LAI less than 4) while agreement was slightly larger than 20% at site 14 with LAI of 5.6 (Fig. 3). The gross estimates indicate that most of $fTPAR(\theta_s)$ is explained by LAI, leaf angle distribution and sky PAR components. Model estimates of $fTPAR(\theta_s)$ decrease with increasing solar zenith angle as was observed at FIFE-89 and KUREX-91 site 12 (as was observed for wheat at limited solar zenith angles (Richardson & Wiegand, 1989)). The results were contrary to measured values at KUREX site 14 (see Figure 2), especially at large solar zenith angles. Scattering of PAR by canopy elements may be a particularly important component of the interaction not represented in the simple model, especially at large LAI. Wheat canopy of large LAI resulted in small $fTPAR$ regardless of sky condition indicating LAI is of great importance at full cover (Hipps *et al.*, 1983).

Spectral vegetation indices varied with solar and view zenith angles (see also Eck & Deering, this issue) as found elsewhere (Wardley, 1984; Shibayama *et al.*, 1987; Deering & Middleton, 1990; Middleton, 1991). NDVIs were symmetrical about nadir for KUREX-91 site 14 while those for KUREX-91 site 12 and FIFE-89 sites 906 and 911 were asymmetrical about nadir (Fig. 4). Values of NDVI derived from BRFs varied in value from approximately 0.70 to 0.85 for KUREX-91 site 14 data while the NDVI values for KUREX-91 site 12 varied from 0.65 to 0.80 (Fig. 4a). Values of NDVI varied in value from 0.60 to 0.85 and 0.55 and 0.75 at FIFE-89 sites 911 and 906, respectively (Fig. 4b). SR and SAVI values varied in a similar manner.

Relationships between $fAPAR(\theta_s)$ and SVIs derived from various BRFs were not consistent over illumination and view angles (Fig. 5) as has been shown in alfalfa (Walter-Shea *et al.*, 1993a), prairie (Walter-Shea *et al.*, 1992) and through modeling exercises (Asrar *et al.*, 1992). Nadir-derived NDVI generally increased as $fAPAR(\theta_s)$ increased at FIFE and was fairly constant at high LAI at the KUREX-91 site 14. Connecting the nadir values across experiments gives a "continuum" of $fAPAR$ yielding an expected pattern of NDVI increasing as $fAPAR$ increases which saturates at high $fAPAR(\theta_s)$. Note that the NDVI value at the largest $fAPAR$ value at FIFE-89 (0.55) was similar to the NDVI value at the largest $fAPAR$ value at KUREX-91 (0.95). SAVI yields a more reasonable contrast in indices from these two experimental sites. Also, angular effects in SAVI as a function of $fAPAR$ appear reduced. If *a priori* information on LAI of the sites is known, the separation between SAVI at the sites would be greater since the adjustment factor would equal 1 for KUREX-91 sites (SAVI would be equal to NDVI). Similar trends as with NDVI occur with SR.

In summary, reflected PAR was similar in magnitude and diurnal variation at selected FIFE-89 and KUREX-91 sites. However, the diurnal variation in transmitted PAR fraction varied considerably between the two research sites and was a dominant component at the FIFE-89 sites. As a result, fAPAR at KUREX-91 decreased with increasing solar zenith angle or remained constant while fAPAR at FIFE-89 increased. Leaf area index, leaf angle distribution and the direct and diffuse sky components explained the majority of transmitted PAR as determined through a simple canopy radiative transfer model. Results indicated scattering of PAR by canopy elements may be an important component in radiation penetration, particularly at large LAI and large solar zenith angles. Spectral vegetation indices varied as a function of fAPAR according to LAI and view zenith angle. NDVI and SR values at FIFE-89 and KUREX-91 were similar in magnitude even though LAI and fAPAR were quite different between the sites. Expected separation in spectral vegetation indices between sites occurred using SAVI. Background effects are of particular concern in estimating LAI and fAPAR using remote sensing in areas of incomplete vegetative cover.

ACKNOWLEDGEMENTS

This work was supported by the National Aeronautics and Space Administration under Grant Nos. NAG5-1762 and NAG5-894. We especially wish to thank our Russian colleagues for their assistance during the field experiment and to Rangasayi Halthore for compiling the input parameters for the 5S atmospheric radiative transfer model and for executing the model.

REFERENCES

- Asrar, G., Myneni, R.B. and Choudhury, B.J. 1992. Spatial heterogeneity in vegetation canopies and remote sensing of absorbed photosynthetically active radiation: A modeling study. *Remote Sens. Environ.*, **41**:85-103.
- Asrar, G., Fuchs, M., Kanemasu, E.T. and Hatfield, J.L. 1984. Estimating absorbed photosynthetic radiation and leaf area index from spectral reflectance in wheat. *Agron. J.*, **76**: 300-306.
- Bartlett, D.S., Whiting, G.J. and Hartman, J.M. 1990. Use of vegetation indices to estimate intercepted solar radiation and net carbon dioxide exchange of a grass canopy. *Remote Sens. Environ.*, **30**:115-128.
- Bauer, M.E., Robinson, B.F., Daughtry, C.S.T. and Biehl, L.L. 1981. Field measurement workshop, Oct. 14-16. Laboratory of Applications of Remote Sensing, Purdue Univ., Lafayette, IN.
- Deering, D.W. and Leone, P. 1986. A sphere-scanning radiometer for rapid directional measurements of sky and ground radiance. *Remote Sens. Environ.*, **10**:1-24.

- Deering, D.W. and Middleton, E.M. 1990. Spectral bidirectional reflectance and effects on vegetation indices for a prairie grassland. In: *Proc. of the Amer. Meteorol. Soc. Symp. on FIFE*, Anaheim, Calif., Febr. 7-9, pp. 71-76.
- Eck, T.F and Deering, D.W. 1993. Spectral bidirectional hemispherical reflectance characteristics of selected sites in the Streletskaya Steppe. *Remote Sens. Rev.*, this issue
- Fritschen, L.J. 1993. Energy and radiation balance components for three grass surfaces near Kursk, Russia. *Remote Sens. Rev.*, this issue.
- Fuchs, M., Asrar, G., Kanemasu, E.T. and Hipps, L.E. 1984. Leaf area estimates from measurements of photosynthetically active radiation in wheat canopies. *Agric. and For. Meteorol.*, **32**: 13-22.
- Halthore, R., Deering, D.W., Markham, B.L., Kozoderov, V.V., Nexval, E. and Shljakhova, L. 1993. Sun-photometric measurements of atmospheric optical properties and atmospheric correction of remotely sensed data during KUREX-91. *Remote Sens. Rev.*, this issue.
- Hipps, L.E., Asrar, G. and Kanemasu, E.T. 1983. Assessing the interception of photosynthetically active radiation in winter wheat. *Agric. Meteorol.*, **28**: 253-259.

- Huete, A.R. 1988. A soil-adjusted vegetation index (SAVI). *Remote Sens. Environ.*, **25**:295-309.
- Jackson, R.D., Moran, M.S., Slater, P.N. and Biggar, S.F. 1987. Field calibration of reference reflectance panels. *Remote Sens. Environ.*, **22**:145-158.
- Markham, B.L., Wood, F.M. and Ahmad, S.P. 1988. Radiometric calibration of the reflective bands of NS-001 thematic mapper simulator (TMS) and modular multispectral radiometer (MMR). *SPIE Recent Advances in Sensors, Radiometers and Data Processing for Remote Sensing*, **924**:96-108.
- Mesarch, M.A., Walter-Shea, E.A., Blad, B.L., Hays, C.J. and Middleton, E.M. 1993. Comparing biophysical properties of the Streletskaya Steppe Reserve and the Konza Prairie. *Remote Sens. Rev.*, this issue.
- Middleton, E.M. 1991. Solar zenith angle effects on vegetation indices and estimation of canopy variables in a tallgrass prairie. *Remote Sens. Environ.*, **38**:45-62.
- Pinter, P.J. Jr. 1993. Solar angle independence in the relationship between absorbed PAR and remotely sensed data for alfalfa. *Remote Sens. Environ.*, (in press)

- Pinter, P.J., Jr., Zipoli, G., Maracchi, G. and Reginato, R.J. 1987. Influence of topography and sensor view angles on NIR/Red ratio and greenness vegetation indices of wheat. *Intl. J. Remote Sens.*, **8**:953-957.
- Richardson, A.J. and Wiegand, C.L. 1989. Canopy leaf display effects on absorbed, transmitted, and reflected solar radiation. *Remote Sens. Environ.*, **29**:15-24.
- Robinson, B.F. and Biehl, L.L. 1979. Calibration procedures for measurement of reflectance factor in remote sensing field research. *SPIE*, **196**:16-26.
- Sellers, P.J. 1985. Canopy reflectance, photosynthesis and transpiration. *Internat. J. of Remote Sens.*, **6**: 1335-1372.
- Shibayama, M., Wiegand, C.L. and Richardson, A.J. 1986. Diurnal patterns of bidirectional vegetation indices for wheat canopies. *Intl. J. Remote Sens.*, **7**:233-246.
- Steven, M. 1977. Standard distributions of clear sky radiance. *Quart. J. Royal Meteorol. Soc.*, **103**:457-465.
- Walter-Shea, E.A., Blad, B.L., Hays, C.J., Mesarch, M.A., Deering, D.W. and Middleton, E.M. 1992. Biophysical properties affecting vegetative canopy reflectance and absorbed

photosynthetically active radiation at the FIFE site. *J. of Geophys. Res.-Atm.* **97**: 18,925-18,934.

Walter-Shea, E.A., Cornell, D., Mesarch, M.A. and Hays, C.J. 1993a. Sun-view geometry effects on absorbed radiation and leaf area estimates in alfalfa. *Remote Sens. Environ.*, (submitted).

Walter-Shea, E.A., Hays, C.J., Mesarch, M.A. and Jackson, R.D. 1993b. An improved goniometer system for calibrating field reference-reflectance panels. *Remote Sens. Environ.*, **43**:131-138.

Wardley, N.W. 1984. Vegetation index variability as a function of viewing geometry. *Intl. J. Remote Sens.*, **5**:861-870.

List of Figures

Figure 1. Instantaneous fraction of absorbed photosynthetically active radiation (fAPAR) as a function of solar zenith angle for FIFE-89 Konza prairie sites 906 (August 6) and 911 (July 28, August 4, and August 8) and KUREX-91 steppe sites 12 (July 14) and 14 (July 20 and 21). Lines represent regression fit to the data.

Figure 2. Instantaneous fractions of reflected and transmitted PAR (fRPAR and fTPAR, respectively) as a function of solar zenith angle for FIFE-89 Konza Prairie site 906 and 911 and KUREX-91 steppe sites 12 and 14. Closed symbols represent fRPAR and open symbols represent fTPAR. Solid line indicates near-continuous fTPAR measured by two sensors mounted near the soil surface at site 14.

Figure 3. Comparison of estimated and measured instantaneous fraction of transmitted photosynthetically active radiation [fTPAR(θ_s)] for FIFE-89 sites 906 and 911 and KUREX-91 sites 12 and 14. Lines represent regression fit to the data.

Figure 4. Normalized Difference Vegetation Index (NDVI) calculated from bidirectional reflectance factors as a function of view and solar zenith angles. a) KUREX-91 sites 12 and 14. b) FIFE-89 sites 906 and 911. Positive view zenith angles represent view angles in the backscatter direction, negative view zenith angles represent view angles in the forward scatter direction.

Figure 5. Spectral vegetation indices calculated from bidirectional reflectance factors as a function of instantaneous fraction of absorbed photosynthetically active radiation in the backscatter, forward scatter and nadir direction. Spectral vegetation indices at large fAPAR are from KUREX sites. a) Normalized Difference Vegetation Index (NDVI) and Soil Adjusted Vegetation Index (SAVI). Closed symbols represent NDVI, open symbols represent SAVI. b) Simple Ratio (SR) Vegetation Index.

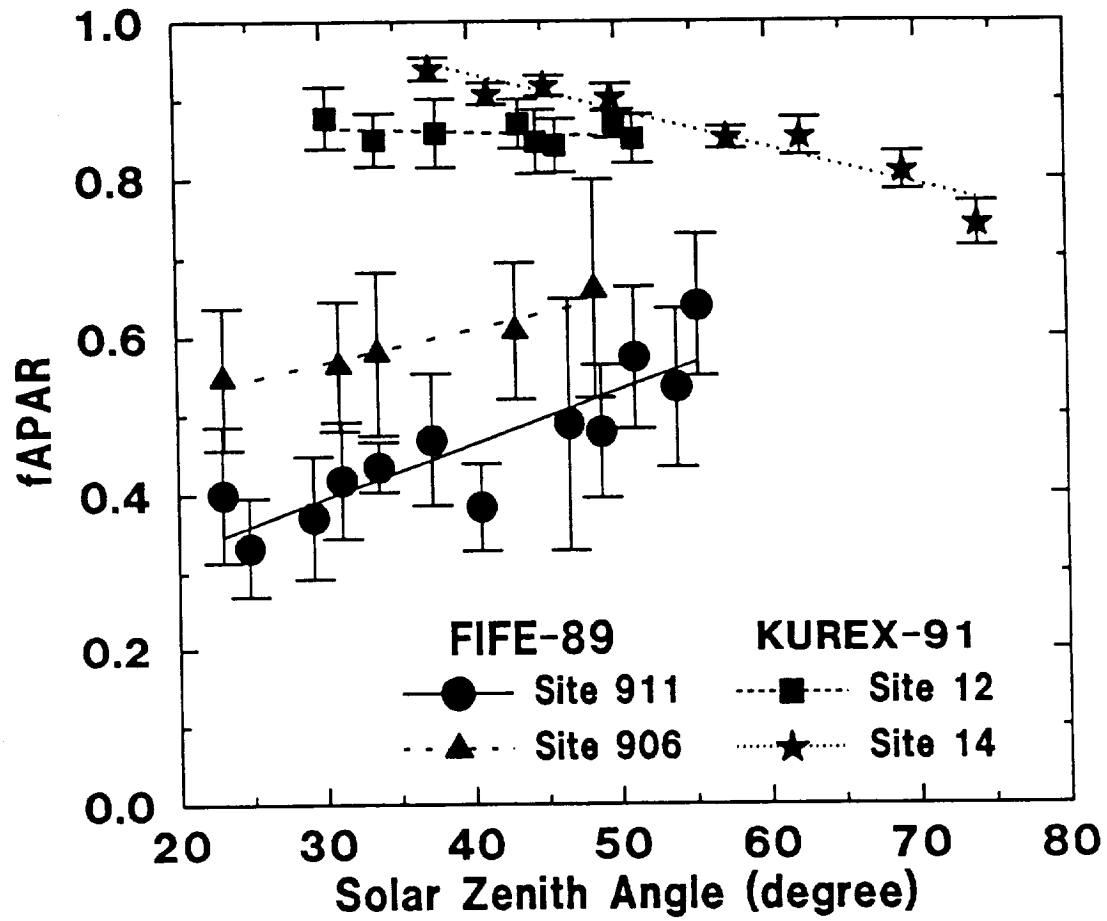


Figure 1

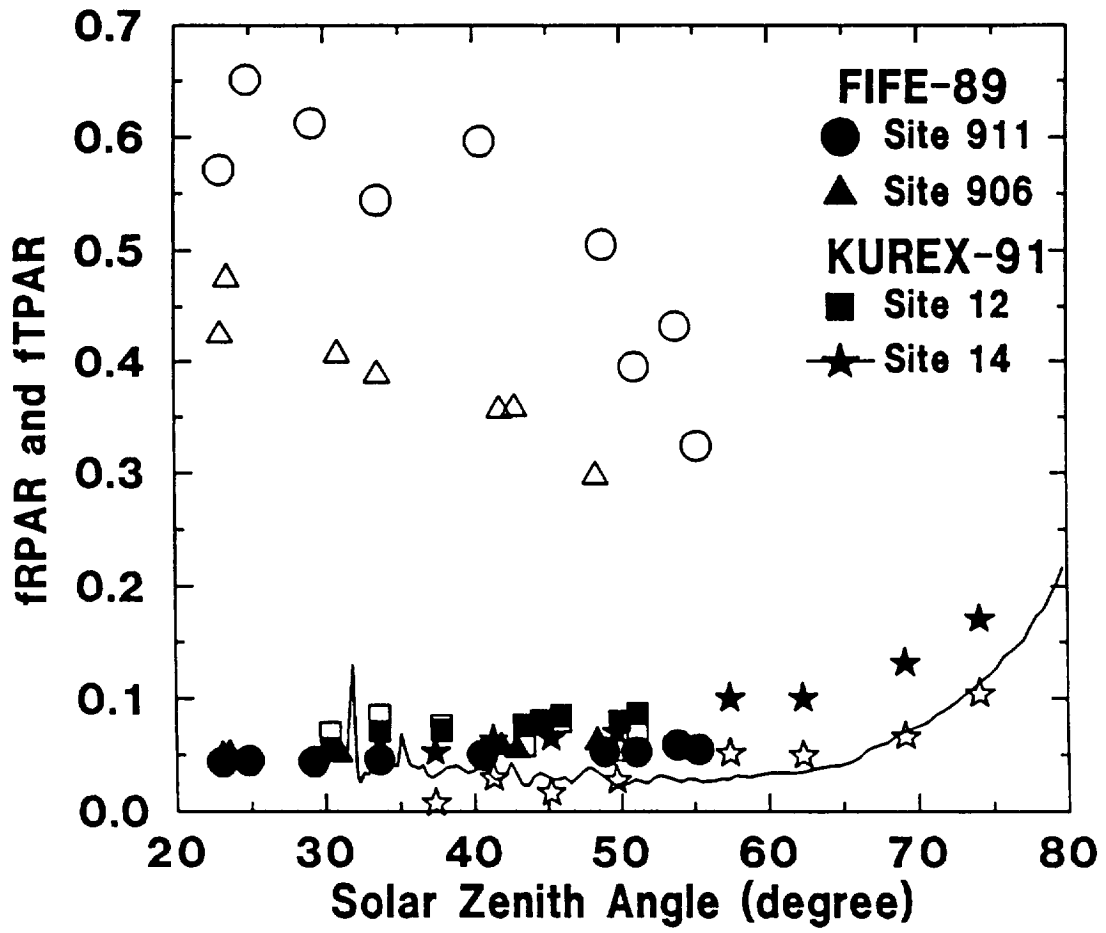


Figure 2

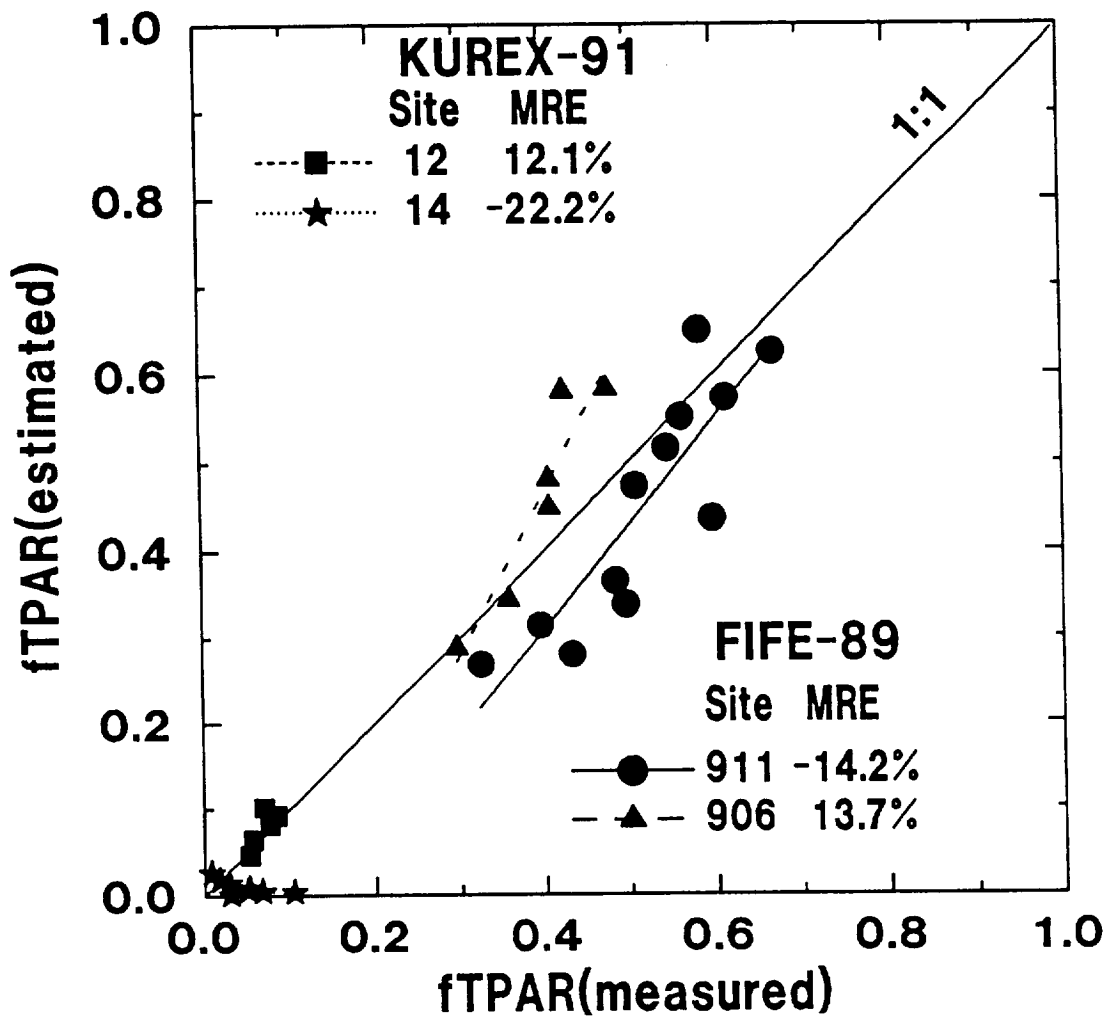
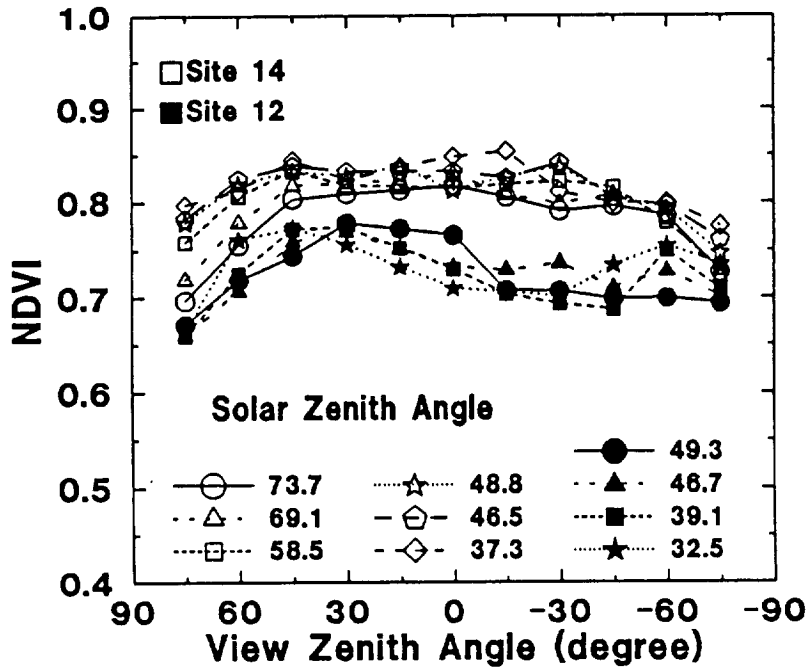


Figure 3

a)



b)

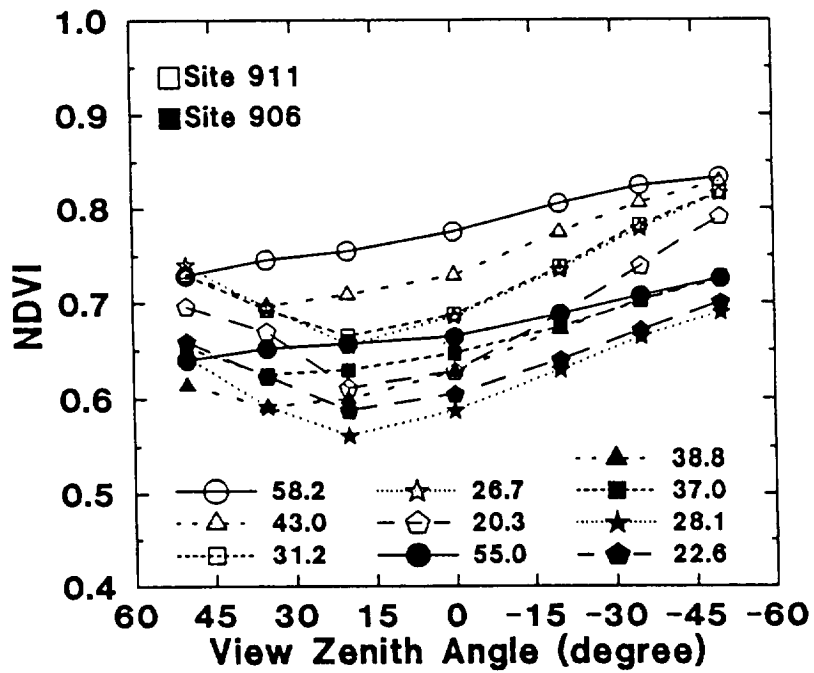
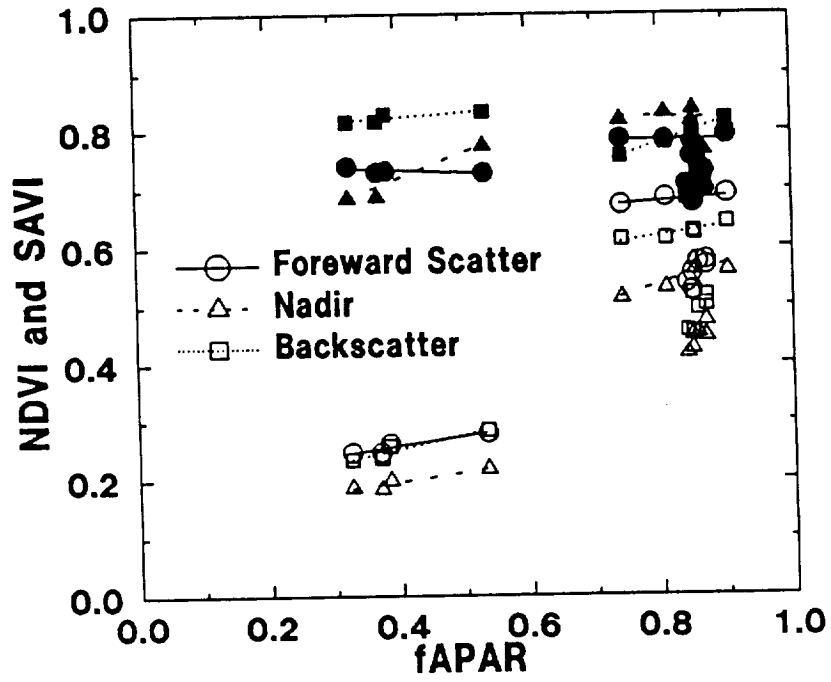


Figure 4

a)



b)

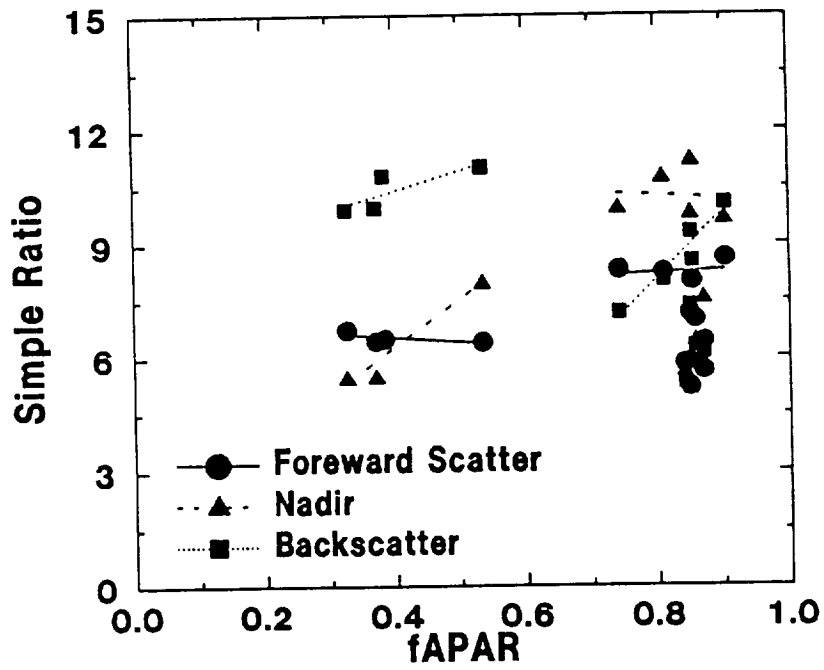


Figure 5

Estimating Emitted Longwave Components of the Radiation Balance in the KUREX-91 and FIFE Studies¹

P.J. Starks*
USDA-ARS
National Agriculture Water Quality Laboratory
Durant, OK

B.L. Blad, E.A. Walter-Shea, C.J. Hays and M.A. Mesarch
Department of Agricultural Meteorology
University of Nebraska, Lincoln, NE

ABSTRACT

key words (up to 6)

INTRODUCTION

Net radiation (R_n) is the balance of the incoming (\downarrow) and outgoing (\uparrow) shortwave radiation ($0.3 \mu\text{m}$ - $3.0 \mu\text{m}$) and longwave radiation (3.0 - $100 \mu\text{m}$) streams

$$R_n = R_{s\downarrow} - R_{s\uparrow} + R_{l\downarrow} - R_{l\uparrow}, \quad (1)$$

where R_s is the shortwave radiation and R_l is the longwave radiation. Net radiation is the quantity of energy available at the earth's surface to drive the processes of photosynthesis, heating of the air and soil, the evaporation of water and miscellaneous processes such as respiration (Rosenberg *et al.*, 1983).

Thermal infrared scanners and hand-held infrared thermometers (IRTs) have been used to measure plant canopy and surface temperatures (*e.g.*, Fuchs and Tanner, 1966; Blad and

* Address correspondence to Dr. P.J. Starks, USDA-ARS, National Agriculture Water Quality Laboratory, PO Box 1430, Durant, OK 74702

¹Published as Paper No. _____, J. Ser., Nebraska Agric. Res. Div.

Received _____ 1993, revised _____.

Rosenberg, 1976; Pinter and Reginato, 1982; Jackson, 1983; Hatfield *et al.*, 1984). For most remote sensing applications, earth surface features are assumed to be opaque to thermal radiation so that its transmissivity is equal to zero (Lillesand and Kiefer, 1979). Good estimates of total outgoing thermal radiation (hemispherical) using IRTs with restricted fields of view can be obtained if the IRT view zenith angle is about 40-45 degrees (Vining and Blad, 1990).

The objective of this paper is to evaluate various methods for estimating the latter two terms in equation (1), especially the $Rl \uparrow$ term, and determine those methods which provide the best estimates of these longwave streams. In a companion paper (Blad *et al.*, 1993) values of the longwave balance obtained with the best methods as determined in this study are combined with the shortwave balance fluxes [the first two terms on the right-hand side to equation (1)] to give estimates of R_n . Jackson *et al.* (1985) estimated $Rl \uparrow$ in Eq. (1) using remotely sensed data and estimated $Rl \downarrow$ with Brutsaert's (1975) equation

$$Rl \downarrow = (\sigma T^4) [1.24(e_0/T)^{17}], \quad (2)$$

where σ is the Stefan-Boltzmann constant, T is the air temperature (K) and e_0 is the actual vapor pressure of the atmosphere. Using the values of the longwave radiation streams estimated in this manner in combination with estimates of the shortwave radiation balance, Jackson *et al.* obtained estimates of R_n that were in close agreement with measure values.

EXPERIMENTAL SITES AND METHODS

The research reported herein was conducted as part of a NASA sponsored experiment known as FIFE (First ISLSCP Field Experiment; see Sellers *et al.*, 1988), which was conducted on or near the Konza Prairie in Kansas during the growing seasons of 1987, 1988 and 1989; and

the KUREX-91 experiment conducted on the Streletskaya Steppe Reserve in Russia during July 1991.

FIFE was initiated in the late spring/early summer of 1987. Based upon vegetative phenology, four intensive field measurement and data collection periods were conducted in 1987. We also collected data between the 1987 intensive field campaigns (IFCs) during May, July, and August of 1988, and during July and August in 1989.

The KUREX-91 experiment was conducted during July 1991 with data being collected from two grassland sites—one mowed in 1987 but not 1990 or 1991, and a second site which had not been mowed for several years.

A calibrated, eight-channel Barnes Modular Multiband Radiometer (MMR) Model 12-1000 (Robinson *et al.*, 1982) was used during the FIFE studies to collect emitted radiation from the surfaces of observation. Channel 8 of the MMR recorded emitted longwave radiation in the 10.4 μm -12.5 μm region. Thermal calibration of the MMR was performed prior to and after data collection in 1987 according to Jackson *et al.* (1983), and after the experimental period in 1988. A specially designed portable mast held the MMR approximately 3.1 m above the soil surface. The MMR, with a field-of-view (FOV) of 15°, produced a circular view spot with a diameter of approximately 0.8 m when pointed at nadir. The mast was tilted to collect data from seven view zenith angles, *i.e.*, nadir and 20, 35 and 50° to either side of nadir. The outgoing hemispherical longwave radiation was calculated using the average temperature of the $\pm 35^\circ$ view zenith angles in the solar principal plane.

A Scheduler Plant Stress Monitor, hand-held infrared thermometer (IRT) was used to obtain the directional outgoing thermal radiation during the KUREX-91 study. IRT readings were taken facing the four cardinal compass points in five 2 m x 2 m plots at each site. The IRT was held at an angle of about 45° approximately 1.5 m above the soil surface, and three

readings were taken for each direction. Outgoing hemispherical longwave radiation was calculated using the average of the 12 IRT temperatures taken per plot.

Eppley pyrgeometers, which measure hemispherical longwave radiation in the region 4.0 μm -50.0 μm , were located near the sites where the MMR data were collected. Enz *et al.* (1975) noted that during clear days the dome of the pyrgeometers would absorb solar radiation and radiate longwave to the thermopile causing the pyrgeometer output to be too high. Albrecht *et al.* (1974) noted similar problems. Subsequently, Albrecht and Cox (1977) developed procedures for calibrating the pyrgeometer, thereby improving data quality. Their calibration equation was given as

$$\frac{E}{\eta} = L - \epsilon\sigma Ts^4 + k\sigma(Td^4 - Ts^4), \quad (3)$$

where

- E = sensor output,
- L = incident irradiance,
- σ = Stefan-Boltzmann constant,
- Ts = sink temperature,
- Td = dome temperature,
- ϵ = emissivity of the thermopile,
- η = instrument sensitivity, and
- k = a constant.

k is determined during the calibration, and η is supplied by the factory.

The pyrgeometers used in these studies were calibrated using the procedures of Albrecht and Cox (1977). However, due to equipment and laboratory limitations the values of k were

erroneous so we used a value of $k = 5^2$. The factory supplied value for η and a k of 5 were used in Eq. (3) to calculate incoming longwave radiation.

The incoming longwave models evaluated in this paper, and discussed below, require air temperature and/or actual vapor pressure of the air. During the FIFE and KUREX-91 studies, these parameters were measured with a Scheduler Plant Water Stress Monitor, a modified and enhanced hand-held infrared thermometer manufactured by the Carborundum Company of Solon, Ohio. Random checks of the parameters measured with the Scheduler were made against measurements made with other instruments during experimental periods and were found to show good agreement.

Estimates of $RI\downarrow$

Several researchers have developed empirical and/or theoretical formulae to estimate incoming longwave radiation. These formulae, generally, require that one or more of the following be known: 1) fraction of cloud cover, 2) air temperature at shelter height, 3) vapor pressure at shelter height, 4) elevation of surface above mean sea level, and 5) incident solar radiation. Because we collected data only under clear skies, the discussion here is limited to clear sky incoming longwave radiation models.

Brunt (1932) produced a simple algorithm whereby the downward flux of longwave radiation is a function of air temperature (T), in degrees Kelvin (K), and the actual vapor pressure (e_0) in millibars [mb]:

²Smith, Eric. Department of Meteorology, Florida State University, Tallahassee, Florida, personal communication.

$$R_{l\downarrow} = \sigma T^4 (a + b e_o^{1/2}), \quad (4)$$

where **a** and **b** are empirically derived constants. For data pertaining to the northern hemisphere, Brunt found values for **a** and **b** to be 0.52 and 0.065, respectively.

Monteith (1961), in an effort to redefine the constants of the Brunt formula, found

$$R_{l\downarrow} = \sigma T^4 (0.53 + 0.065 e_o^{1/2}). \quad (5)$$

Because the value of **b** is the same in (3) and (4) and **a** differs only by one one-hundredth, we used

$$R_{l\downarrow} = \sigma T^4 (0.525 + 0.065 e_o^{1/2}), \quad (6)$$

a reasonable compromise.

Brutsaert (1975) analytically derived an equation (Eq. 2) for atmospheric emissivity which was used to estimate clear-sky incoming longwave radiation. This equation incorporates both e_o and T .

Swinbank (1963) believed that the importance of water vapor's contribution to longwave radiation was exaggerated. With this premise in mind, he developed an equation to estimate incoming longwave radiation based only on air temperature at shelter height. This equation is

$$R_{l\downarrow} = (5.31 \times 10^{-14}) (T^6). \quad (7)$$

Swinbank's work has received some criticism for being too empirical and not taking into account a wider range of atmospheric conditions (Discussion, 1964), among other concerns.

Deacon (1970) showed that Eq. (7) could be derived from the knowledge of atmospheric emission. Additionally, he suggested that the value obtained from Eq. (7) should be adjusted to account for atmospheric pressure at the point of observation. This correction takes the form

$$R\downarrow = R_{sb} - 0.035(z/1000)\sigma T^4 \quad (8)$$

where R_{sb} is the value obtained from Eq. (7) and z is the height of the station above mean sea level in meters.

Paltridge (1970) further suggested that the values obtained from the formula of Swinbank would be too high during the day because of a bias in Swinbank's model towards inversion conditions. Comparison of measured incoming longwave to values derived from Eq. (7) led Paltridge to state that it overestimated by about 30 Wm^{-2} for hourly averages.

Idso and Jackson (1969), like Swinbank, developed a procedure for calculating incoming longwave radiation based only upon screen-level air temperatures. Their equation was developed from a wider range of air temperatures than that of Swinbank. Idso and Jackson wrote their equation as

$$R\downarrow = \sigma T^4 [1 - c(\exp - d(273 - T)^2)], \quad (9)$$

where $c = 0.261$ and $d = 7.77 \times 10^{-4}$.

Aase and Idso (1978) compared Eq. (9) to the formula of Brutsaert for the purpose of evaluating the performance of each at temperatures lower than 0°C . Using daily averages of air temperature and humidity obtained at Sidney, Montana it was observed that the Brutsaert method always underestimated the true value while that of Idso and Jackson underestimated, matched, and then overestimated $R\downarrow$ as the air temperature went from 0° to -37°C . These findings led

Satterlund (1979) to suggest an equation for better prediction of incoming longwave with extremes in air temperature and humidity. Using the data sets of Aase and Idso (1978) and Stoll and Hardy (1955) he developed the following empirical equation:

$$RL\downarrow = (\sigma T^4) (1.08) [1 - \exp(-e_o^{T/2016})] \quad (10)$$

Satterlund compared results from Eq. (10), using the data sets of Aase and Idso (1978) and Stoll and Hardy (1955), to the results obtained from the algorithms supplied by Brutsaert (1975) and Idso and Jackson (1969). He found that Eq. (10) gave the best fit to the data.

Idso (1981) noted that several of the longwave equations (Brunt, Swinbank, Idso and Jackson, Brutsaert) did not compare well at all times, particularly when the air temperature fell below 273 K. He further noted that work on atmospheric water vapor dimers may explain why these particular longwave models do not compare well to measured values at all air temperatures. Therefore, Idso sought to provide a longwave model based upon existing knowledge of absorption/emission in the 8 to 14 μm waveband while incorporating the water dimer hypothesis. Two equations emerged from his work:

$$RL\downarrow = (\sigma T^4) (0.179 e_o^{1/7} \exp(350/T)) \quad (11)$$

$$RL\downarrow = (\sigma T^4) [0.70 + 5.95 \times 10^{-5} e_o \exp(1500/T)] \quad (12)$$

Air temperature and/or actual vapor pressure measurements are needed in the above equations. The Scheduler records air temperature and vapor pressure deficit (VPD). If air

temperature and VPD are known, then actual vapor pressure can be determined in the following way

$$e_o = (6.108) (10^{a/b}) - VPD \quad (13)$$

where

$$\begin{aligned} e_o &= \text{actual vapor pressure [mb]} \\ a &= (7.5) (T) \\ b &= 237.3 + T \end{aligned}$$

and T is the air temperature in °C. The VPD as given by the Scheduler is in units of kPa and is converted into units of [mb] by multiplying by 10 before use in Eq. (13).

Equation (13) was used to estimate actual vapor pressure for the FIFE 1987, 1989 and KUREX-91 data sets, and for four of seven days of the 1988 data set. Due to equipment problems Scheduler data were not available for the other three days of data collection in 1988 so an alternate data source was used. For these days dry (Td) and wet (Tw) bulb temperatures, measured at a height of approximately two meters on Portable Automated Mesonet (PAM) stations, were used. Wet and dry bulb temperatures can be used to calculate estimates of e_o from

$$e_o = e_s - AP(Td - Tw) \quad (14)$$

where

$$e_s = 6.108 (10^{a/b}) \quad (15)$$

$$A = 6.6 \cdot 10^{-4} (1 + 1.15 \cdot 10^{-3} \cdot T_w) \quad (16)$$

A is in units of $^{\circ}\text{C}^{-1}$, and a and b are defined in Eq. (13). P is a pressure term, and for this study was set equal to 966 mb.

Statistical Methods

Willmott and Wicks (1980) and Willmott (1981, 1982) raised concerns about the exclusive use of r and r^2 in the context of model performance evaluation. Willmott (1981) noted that very dissimilar values of estimates and measurements can produce an r very near one. Moreover, small differences between measured and estimated quantities can produce a low or even negative r (Willmott and Wicks, 1980). A statistical parameter, the d index of model agreement, was proposed by Willmott (1982). Used in conjunction with other common statistical measures, d aids in evaluating the accuracy of models. A $d=1$ indicates complete agreement between modeled and measured values, a $d=0$ indicates complete disagreement.

Mean bias errors (MBE) describe the average deviation of the predicted values from the measured values. Root mean square errors (RMSE) describe the average total error in the estimating procedure and can be partitioned into a random or unsystematic component (E_u) and a systematic component (E_s).

Unsystematic errors may occur because of unobserved intermittent instrument problems, inconsistent data collection techniques, or random variations in the phenomena being observed. These random errors can be visualized as a measure of clustering about a regression line drawn through a cloud of points. Large random errors would occur if data points were greatly dispersed and small random errors if points were tightly clustered about the regression line.

Systematic errors may arise due to consistent error in experimental procedure, instrument calibration error, or in the predicting equation. These errors may be thought of as the distance from the one-to-one line to the regression line. If the distance is large, there is a large systematic error, while a small error indicates the two lines are in close proximity.

Mean relative error (MRE) is the average percentage that the estimates over or under predict relative to the measured values.

RESULTS

Equations (2) and (6-12) were used to compute estimates of incoming longwave radiation. Values of incoming longwave radiation estimated with Eqs. (7) (Swinbank's model) and (8) (Deacon's model) were reduced by 30 Wm^{-2} based upon the suggestion of Paltridge (19770), and will be referred to as MSw and MDc, respectively. The results from the ten algorithms were compared to simultaneously measured values recorded by the pyrgeometers, located nearby.

Estimates derived from the incoming longwave radiation models were compared to measured values and statistically analyzed for the 1987 (Table 1) and 1988 (Table 2) data sets. Comparison of the information in Tables 1 and 2 indicates that all models performed better in 1988 than in 1987, as manifested by the d , r , and r^2 statistics. Eq. (12) shows the largest MBE in both years and MSw and MDc exhibit the smallest. Most of the models have an MRE of less than 10%, exceptions being Eq. (9) and (12) in 1987 and Eqs. (2) and (12) in 1988. Eq. (10) possesses the largest RMSE in both years while the MSw and MDc models have the lowest, for both 1987 and 1988. The random error (E_u) is small and lies between 10 Wm^{-2} and 20 Wm^{-2} for all models in both data sets. However, the systematic error (E_s) is large for all models, except for MSw and MDc. In these two cases E_u is two to four times larger than E_s .

In regards to the low biases in MSw and MDc, we should recall that Paltridge (1970) noted a 30 Wm^{-2} overestimation in values produced from Eq. (7). We also note that Eq. (8) is an elevation correction to Eq. (7) and the findings of Paltridge apply equally well to it. Es for Eqs. (7) and (8) is approximately 30 Wm^{-2} for the 1987 data set, and is 33 Wm^{-2} and 26 Wm^{-2} , respectively, for the 1988 data set. Thus, the findings of Paltridge (1970) are corroborated here, as evidenced by the small biases of the MSw and MDc models.

The object behind the evaluation of these longwave radiation models is to find one that will consistently yield acceptable estimates of $\text{RI}\downarrow$. Of those models evaluated, the MDc model performed best overall—a model which requires only air temperature and station elevation as input. If the elevation information is not available, the MSw model would also work well. Except for Eq. (11), the models using e_0 and T did not perform as well as Eq. (6) or MDc. Idso (1981) expressed some reservations about the use of Eq. (11) and suggested that Eq. (12) is generally more useful.

DISCUSSION

We noted above that the $\text{RI}\downarrow$ models performed better in 1988 than in 1987. An obvious question is why? First, we recall that the 1987 $\text{RI}\downarrow$ estimates were all derived from input obtained from the Scheduler, whereas part of the 1988 $\text{RI}\downarrow$ estimates were derived from wet and dry bulb temperatures measured at PAM stations. We separated the 1988 $\text{RI}\downarrow$ estimates into those obtained via PAM input and those using Scheduler data, and statistically analyzed them (Table 3). From Table 3 it is observed that each d statistic is lower for each model, in each of the two separate cases, than when all the data are combined (Table 2). Thus, there is a synergism when the PAM-derived $\text{RI}\downarrow$ estimates are combined with those derived from the Scheduler data. We further observe that the PAM-derived estimates are generally further away

from their measured mean, as indicated by MBE and E_s , than are their Scheduler-derived counterparts. Additionally, the measured mean for the PAM data set is approximately 36 Wm^{-2} lower than the measured mean for the total data set (Table 2), but the measured mean for the Scheduler portion of the data set is approximately 24 Wm^{-2} higher. There appear to be compensating errors in the 1988 total data set which give rise to higher d and r statistics, than those of the 1987 data set. As a final note in these regards, we note that the d statistics for the Scheduler portion of the 1988 data set are more in line with those of the 1987 data set than those d statistics from the PAM-derived portion.

Except for Eq. (12), E_s varies little between the 1987 and 1988 $R_{l\downarrow}$ data sets, particularly if we only consider the Scheduler portion of the 1988 data set. Therefore, we suggest that estimates derived from Eqs. (2), (6), and (9-12) be reduced by the amounts shown in Table 4.

Based on results from the 1987 and 1988 FIFE studies, a subset of the models was evaluated using FIFE-89 and KUREX-91 data. The statistical information on the performance of those models is given in Table 3.

The Brunt model gave the best estimates of incoming longwave radiation for the KUREX-91 data set, while the Deacon, modified Swinbank, and Brunt models all performed well using the FIFE-89 data. Using this information, the Brunt model was selected to estimate the incoming longwave radiation streams for use in estimating the net radiation. The model outputs were not adjusted by subtracting the 30 Wm^{-2} bias error, as shown in Table 4.

The modeled incoming longwave radiation flux densities for the FIFE-89 and KUREX-91 are plotted against the measured incoming longwave in Figure 1. There is good agreement between the measured and modeled values. The KUREX-91 data tended to cluster around the 1:1 line, but were restricted to a narrow range of $R_{l\downarrow}$ values, ranging from about 280 to 350

Wm^{-2} . The FIFE-89 data covered a much wider range of $\text{RI}\downarrow$ values and showed a distinct tendency for the modeled values to overestimate $\text{RI}\downarrow$ compared to the measured values, especially at the higher $\text{RI}\downarrow$ flux densities. Adjusting the data by subtracting 30 Wm^{-2} would have brought the FIFE-89 modeled and measured values into closer agreement, but would have caused the model values for the KUREX-91 study to underestimate the $\text{RI}\downarrow$ flux densities.

To complete the longwave radiation balance for the FIFE-89 and KUREX-91 studies, the outgoing longwave radiation flux densities were calculated from the surface temperature data. The results are shown in Fig. 2 and in Table 6. There is very good agreement between the measured and estimated values (MRE of 1 and 2% for the KUREX-91 and FIFE-89 data, respectively), especially at flux densities between 375 and 450 Wm^{-2} .

The results of these studies suggest that the components of the longwave radiation balance can be adequately estimated using the Brunt equation for estimating $\text{RI}\downarrow$ and the surface temperatures measured by IRTs with view zenith angles of 35-45°.

ACKNOWLEDGEMENTS

This work was performed under NASA Contract NAG 5-894. The authors would like to thank Dr. Elizabeth A. Walter-Shea, Cindy Hays, Roel Vining, Dave Klazinski, Doug Eschelbrenner, Pedro Zara, Greg Grosshans, Mark Mesarch, and Vicki Samson for their help in collecting the field data. Our thanks are also extended to NCAR for providing the PAM data. The corresponding author thanks Dr. Wayne Decker for allowing him to write this paper while working in his Postdoctoral position at the Cooperative Institute for Applied Meteorology at the University of Missouri, Columbia, Missouri.

BIBLIOGRAPHY

Aase, J.K. and Idso, S.B. 1978. A comparison of two formula types for calculating long-wave radiation from the atmosphere. *Water Resources Research* **14**:623-625.

Albrecht, B. and Cox, S.K. 1977. Procedures for improving pyrgeometer performance. *J. Appl. Meteorol.* **16**:188-197.

Albrecht, B., Poellet, M., and Cox, S.K. 1974. Pyrgeometer measurements from aircraft. *Rev. of Scientific Instrumentation* **45**:33-38.

Brunt, D. 1932. Notes of radiation in the atmosphere 1. *Quart. J. Royal Meteorol. Soc.* **58**:389-418.

Brutsaert, W. 1975. On a derivable formula for long-wave radiation from clear skies. *Water Resources Research* **11**:742-744.

Daughtry, C.S.T., Kustas, W.P., Moran, M.S., Pinter, P.J., Jackson, R.D., Brown, P.W., Nichols, W.D., and Gay, L.W. 1990. Spectral estimates of net radiation and soil heat flux. *Remote Sens. of Environ.* **32**:111-124.

Deacon, E.L. 1970. The derivation of Swinbank's long-wave radiation formula. *Quart. J. Royal Meteorol. Soc.* **96**:313-319.

Discussion. 1964. Discussion: Long-wave radiation from clear skies by W.C. Swinbank. *Quart. J. Royal Meteorol. Soc.* **90**:488-493.

Enz, J.W., Klink, J.C., and Baker, D.G. 1975. Solar radiation effects on pyrgeometer performance. *J. Appl. Meteorol.* **14**:1297-1302.

Idso, S.B. 1981. A set of equations for full spectrum and 8 to 14 μm and 10.5 to 12.5 μm thermal radiation from cloudless skies. *Water Resources Research* **17**:295-304.

Idso, S.B. and Jackson, R.D. 1969. Thermal radiation from the atmosphere. *J. Geophys. Res.* **74**:5397-5403.

Jackson, R.D., Dusek, D.A., and Ezra, C.E. 1983a. Calibration of the thermal channel on four Barnes Model 12-1000 multi-band radiometers. *United States Water Conservation Laboratory Report 12*, Phoenix, AZ.

Jackson, R.D., Pinter, Jr., P.J., and Reginato, R.J. 1985. Net radiation calculated from remote multispectral and ground station meteorological data. *Agric. Forest Meteorol.* **35**:153-164.

Monteith, J.L. 1961. An empirical method for estimating longwave radiation exchanges in the British Isles. *Quart. J. Royal Meteorol. Soc.* **87**:171-179.

- Moran, M.S., Jackson, R.D., Raymond, L.H., Gay, L.W., and Slater, P.N. 1989. Mapping surface energy balance components by combining Landsat Thematic Mapper and ground-based meteorological data. *Remote Sens. of Environ.* **30**:77-87.
- Paltridge, G.W. 1970. Day-time long-wave radiation from the sky. *Quart. J. Royal Meteorol. Soc.* **96**:645-653.
- Robinson, B.F., Buckley, R.E., and Burgess, J.A. 1982. Performance evaluation and calibration of a modular multiband radiometer for remote sensing field research. Agristars Technical Report SR-P2-04318, Purdue University, Laboratory for Applications of Remote Sensing, West Lafayette, IN.
- Rosenberg, N.J., Blad, B.L., and Verma, S.B. 1983. *Microclimate: The Biological Environment*, 2nd ed. John Wiley and Sons: New York. 495 pp.
- Satterlund, D.R. 1979. An improved equation for estimating long-wave radiation from the atmosphere. *Water Resources Research* **15**:1649-1650.
- Sellers, P.J., Hall, F., Asrar, G., Strebel, D.E., and Murphy, R.E. 1988. The First ISLSCP Field Experiment (FIFE). *Bull. Amer. Meteorol. Soc.* **69**:22-27.
- Starks, P.J. 1990. Measured and modeled radiation fluxes from prairie vegetation at the FIFE study site. Ph.D. Dissertation, University of Nebraska, Lincoln. 179 pp.

- Starks, P.J., Norman, J.M., Blad, B.L., Walter-Shea, E.A., and Walthall, C.L. 1991. Estimation of shortwave hemispherical reflectance (albedo) from bidirectionally reflected radiance data. *Remote Sens. Environ.* **38**:123-134.
- Stoll, A.M. and Hardy, J.D. 1955. Thermal radiation measurements in summer and winter Alaskan climates. *EOS Trans. of the American Geophysical Union* **36**:213-225.
- Swinbank, W.C. 1963. Long-wave radiation from clear skies. *Quart. J. Royal Meteorol. Soc.* **89**:339-348.
- Willmott, C.J. 1981. On the validation of models. *Physical Geographer* **2**:184-194.
- Willmott, C.J. 1982. Some comments on the evaluation of model performance. *Bull. Amer. Meteorol. Soc.* **63**:1309-1313.
- Willmott, C.J. and Wicks, D.E. 1980. An empirical method for the spatial interpolation of monthly precipitation within California. *Physical Geographer* **1**:59-73.

Table 1. Statistics from comparison of various incoming longwave estimations with measured pyrgeometer incoming longwave values using the FIFE-87 data set. N=230.

Model	d	r	r ²	MBE (Wm ⁻²)	MRE (%)	RMSE (Wm ⁻²)	Eu (Wm ⁻²)	Es (Wm ⁻²)	\bar{x} (Wm ⁻²)	s (Wm ⁻²)
FIFE-87										
Brutsaert (Eq. 2)	0.573	0.848	0.719	34.65	9.11	36.59	11.28	34.80	416.70	21.33
Brunt (Eq. 6)	0.689	0.860	0.739	25.56	6.69	28.25	12.15	25.51	407.61	23.83
Swinbank (Eq. 7)	0.512	0.621	0.385	36.93	9.75	36.10	20.68	29.59	418.98	24.51
Mod. Swinbank (MSw)	0.766	0.621	0.385	6.93	1.88	20.83	19.18	8.14	388.98	24.51
Deacon (Eq. 8)	0.574	0.622	0.386	29.74	7.87	35.46	18.99	29.95	411.79	24.28
Mod. Deacon (MDC)	0.779	0.622	0.386	-0.26	-7.73	19.51	18.98	2.54	381.79	24.28
Idso-Jackson (Eq. 9)	0.478	0.620	0.384	41.52	10.95	46.21	19.68	41.81	423.57	25.13
Satterlund (Eq. 10)	0.527	0.758	0.575	36.20	9.57	38.63	12.20	36.66	418.24	18.75
Isdo 1 (Eq. 11)	0.667	0.845	0.715	26.34	6.93	28.64	11.40	26.28	408.39	21.38
Isdo 2 (Eq. 12)	0.446	0.868	0.753	52.83	13.85	54.17	11.79	52.85	434.88	23.75
Measured									382.05	19.62

where $d = 1 - [\Sigma(E-M)^2/\Sigma | E-x | + | M-x |]^2$

r = correlation coefficient

MBE = $N^{-1}\Sigma(E-M)$

MRE = $N^{-1}[\Sigma(E-M)/M][100]$

RMSE = $\{[(N^{-1}\Sigma(P-M)^2) + [N^{-1}\Sigma(P-E)^2]]^{1/2}$

Eu = $(N^{-1}\Sigma(P-E)^2)^{1/2}$

Es = $(N^{-1}\Sigma(P-M)^2)^{1/2}$

\bar{x} = $N^{-1}\Sigma E$ or $N^{-1}\Sigma M$

s = $[(N^{-1})^{-1}\Sigma(E-x)^2]^{1/2}$ or $[(N^{-1})^{-1}\Sigma(M-x)^2]^{1/2}$

P = predicted value from linear regression of estimated and measured values

E = estimated value

M = measured value

x = mean measured value

Table 2. Statistics for comparison of various incoming longwave estimations with measured pyrgeometer incoming longwave values using the FIFE-88 data set. N=70.

Model	d	r	r ²	MBE (Wm ⁻²)	MRE (%)	RMSE (Wm ⁻²)	Eu (Wm ⁻²)	Es (Wm ⁻²)	\bar{x} (Wm ⁻²)	s (Wm ⁻²)
FIFE-88										
Brutsaert (Eq. 2)	0.679	0.914	0.835	43.30	11.36	45.32	12.06	43.68	432.37	29.91
Brunt (Eq. 6)	0.723	0.895	0.802	38.71	10.13	41.42	14.47	38.81	427.79	32.72
Swinbank (Eq. 7)	0.797	0.938	0.880	33.07	8.52	35.77	13.20	33.24	422.14	38.37
Mod. Swinbank (MSw)	0.962	0.938	0.880	3.07	0.75	13.76	13.20	3.87	392.14	38.37
Deacon (Eq. 8)	0.854	0.938	0.880	25.49	6.57	28.72	13.05	25.58	414.57	37.91
Mod. Deacon (MDc)	0.961	0.938	0.880	-4.51	-1.20	13.91	13.05	4.82	384.57	37.91
Idso-Jackson (Eq. 9)	0.766	0.927	0.860	36.63	9.44	39.55	14.42	36.83	425.70	38.78
Satterlund (Eq. 10)	0.728	0.936	0.876	37.00	9.74	39.00	10.06	37.67	426.07	28.79
Idso 1 (Eq. 11)	0.750	0.915	0.837	34.77	9.15	37.18	12.07	35.16	423.85	30.20
Idso 2 (Eq. 12)	0.516	0.832	0.692	70.69	18.51	72.98	16.43	71.11	459.76	29.82
Measured									389.07	33.77

Table 3. 1988 Data Set: Estimates of $R1 \downarrow$ separated into those derived from PAM[®] data (n=28) and those derived from Scheduler[†] data. N=42.

Model	d	r	r ²	MBE (Wm ⁻²)	MRE (%)	RMSE (Wm ⁻²)	Eu (Wm ⁻²)	Es (Wm ⁻²)	\bar{x} (Wm ⁻²)	s (Wm ⁻²)
Brutsaert (Eq. 2)	0.403	0.720	0.518	50.61	14.40	52.38	13.01	50.74	403.53	19.07
	0.457	0.766	0.587	38.42	9.34	39.95	11.35	38.30	451.60	17.87
Brunt (Eq. 6)	0.441	0.720	0.518	44.53	12.65	47.02	15.17	44.51	397.45	22.25
	0.487	0.738	0.545	34.84	8.45	37.34	13.79	34.70	448.01	20.69
Swinbank (Eq. 7)	0.547	0.725	0.526	28.92	8.27	31.17	11.14	29.12	381.84	16.47
	0.490	0.762	0.581	35.83	8.68	38.33	13.59	35.84	449.00	21.24
Mod. Swinbank (MSw)	0.843	0.725	0.526	-1.08	-0.25	12.00	11.14	4.46	351.84	16.47
	0.835	0.762	0.581	5.83	1.41	14.79	13.59	5.84	419.00	21.24
Deacon (Eq. 8)	0.615	0.725	0.526	21.83	6.26	24.74	11.00	22.16	374.75	16.26
	0.572	0.762	0.581	27.94	6.77	30.95	13.43	27.89	441.11	20.99
Mod. Deacon (MDc)	0.794	0.725	0.526	-8.17	-2.26	14.47	11.00	9.40	344.75	16.26
	0.853	0.762	0.581	-2.06	-0.50	13.59	13.43	2.12	411.11	20.99
Idso-Jackson (Eq. 9)	0.520	0.725	0.526	32.37	9.24	34.36	11.61	32.34	385.30	17.16
	0.448	0.706	0.498	39.46	9.57	42.36	15.31	39.51	452.64	21.88
Satterlund (Eq. 10)	0.434	0.722	0.521	43.68	12.47	45.17	10.28	43.99	396.60	15.13
	0.504	0.787	0.620	32.54	7.92	34.10	9.74	32.68	445.71	16.00
Idso 1 (Eq. 11)	0.455	0.720	0.518	41.70	11.87	43.65	13.00	41.68	394.62	19.06
	0.530	0.767	0.589	30.16	7.33	32.35	11.39	30.28	443.33	17.97
Idso 2 (Eq. 12)	0.287	0.718	0.515	82.47	23.40	84.25	16.59	82.60	435.39	24.25
	0.323	0.660	0.435	62.84	15.26	64.82	15.45	62.95	476.01	20.81
Measured		$\bar{x}_{PAM} = 352.92$	$\bar{x}_{SCHED} = 413.17$						$\bar{x}_{ALL} = 389.07$	
		$S_{PAM} = 16.3$	$S_{SCHED} = 16.0$						$S_{ALL} = 33.77$	

[®]PAM statistics in light face print.

[†]Scheduler statistics in bold face print.

Table 4. Overestimates (biases) found in the $R1\downarrow$ models.

Model Name	Equation #	Bias
Brutseart	2	35 Wm^{-2}
Brunt	6	30
Swinbank	7	30
Deacon	8	30
Idso-Jackson	9	40
Satterlund	10	35
Idso 1	11	30
Idso 2	12	60

Table 5. Statistics from comparison of various incoming longwave estimations with measured pyrgeometer incoming longwave values using FIFE-89 and KUREX-91 datasets. $N_{\text{FIFE89}} = 173$ and $N_{\text{KUREX91}} = 55$.

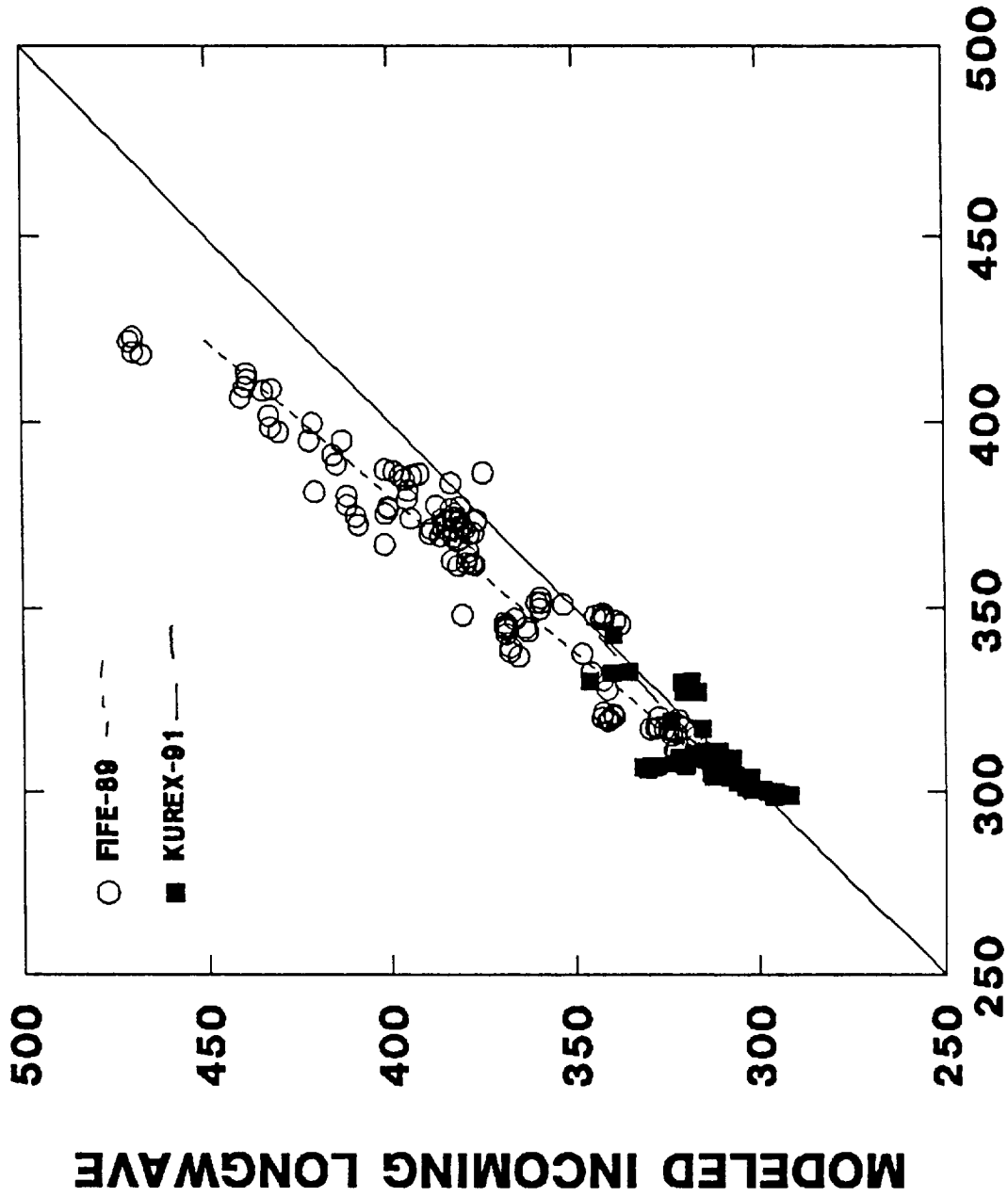
Dataset/ Algorithm	d	r	r ²	MBE Wm ²	MRE %	RMSE Wm ²	Eu Wm ²	Es Wm ²	\bar{x} Wm ²	s Wm ²
KUREX-91										
Brunt (Eq. 6)	0.82	0.74	0.55	4.72	1.53	9.26	9.01	2.13	314.97	12.74
Swinbank (Eq. 7)	0.33	0.63	0.40	42.28	11.04	41.80	9.02	40.81	350.94	14.35
Mod. Swinbank (MSw)	0.66	0.63	0.40	10.68	3.46	15.51	11.04	10.90	320.94	14.35
Deacon (Eq. 8)	0.35	0.63	0.40	38.83	10.97	38.33	9.02	37.25	347.25	14.26
mod. Deacon (MDc)	0.72	0.63	0.40	7.24	2.35	13.23	10.97	7.40	317.49	14.26
Measured									310.26	10.63
FIFE-89										
Brunt (Eq. 6)	0.90	0.95	0.91	16.43	4.46	20.59	10.89	17.47	377.8	35.7
Swinbank (Eq. 7)	0.88	0.94	0.87	0.00	4.96	20.40	9.75	17.94	379.0	27.4
Mod. Swinbank (MSw)	0.92	0.94	0.87	-12.42	-3.39	15.92	9.72	12.61	349.0	27.4
Deacon (Eq. 8)	0.93	0.94	0.87	10.52	3.00	14.48	9.60	10.85	371.9	27.1
Mod. Deacon (MDc)	0.87	0.94	0.87	-19.48	-5.35	22.08	9.60	19.89	341.9	27.1
Measured									361.4	28.5

Table 6. Statistics from comparison of outgoing longwave estimations from the average of off-nadir (35 and 45°) surface temperature measurements changed to units of Wm² with measured pyrgeometer outgoing longwave values using the FIFE-89 MMR and KUREX-91 IRT datasets.

Algorithm	d	r	r ²	MBE Wm ²	MRE %	RMSE Wm ²	Eu Wm ²	Es Wm ²	\bar{x} Wm ²	s Wm ²
KUREX-91	0.94	0.93	0.87	4.50	1.02	10.28	8.60	5.63	430.16	24.00
Measured									425.66	18.89
FIFE-89	0.93	0.94	0.93	10.22	2.10	15.66	10.88	11.26	492.28	37.0
Measured									477.07	25.5

LIST OF FIGURES

- Fig. 1. Flux densities of incoming longwave radiation estimated with the Brunt equation (1932) compared with measured values at FIFE-89 and KUREX-91. The solid line is the 1:1 line.
- Fig. 2. Flux densities of outgoing longwave radiation estimated from average canopy temperatures measured with the MMR thermal channel ($\pm 35^\circ$ view zenith angle in the solar principal plane) at FIFE-89 and with the IRT (Scheduler at 45° view zenith angle in the four cardinal directions) compared with measured values. The solid line is the 1:1 line.

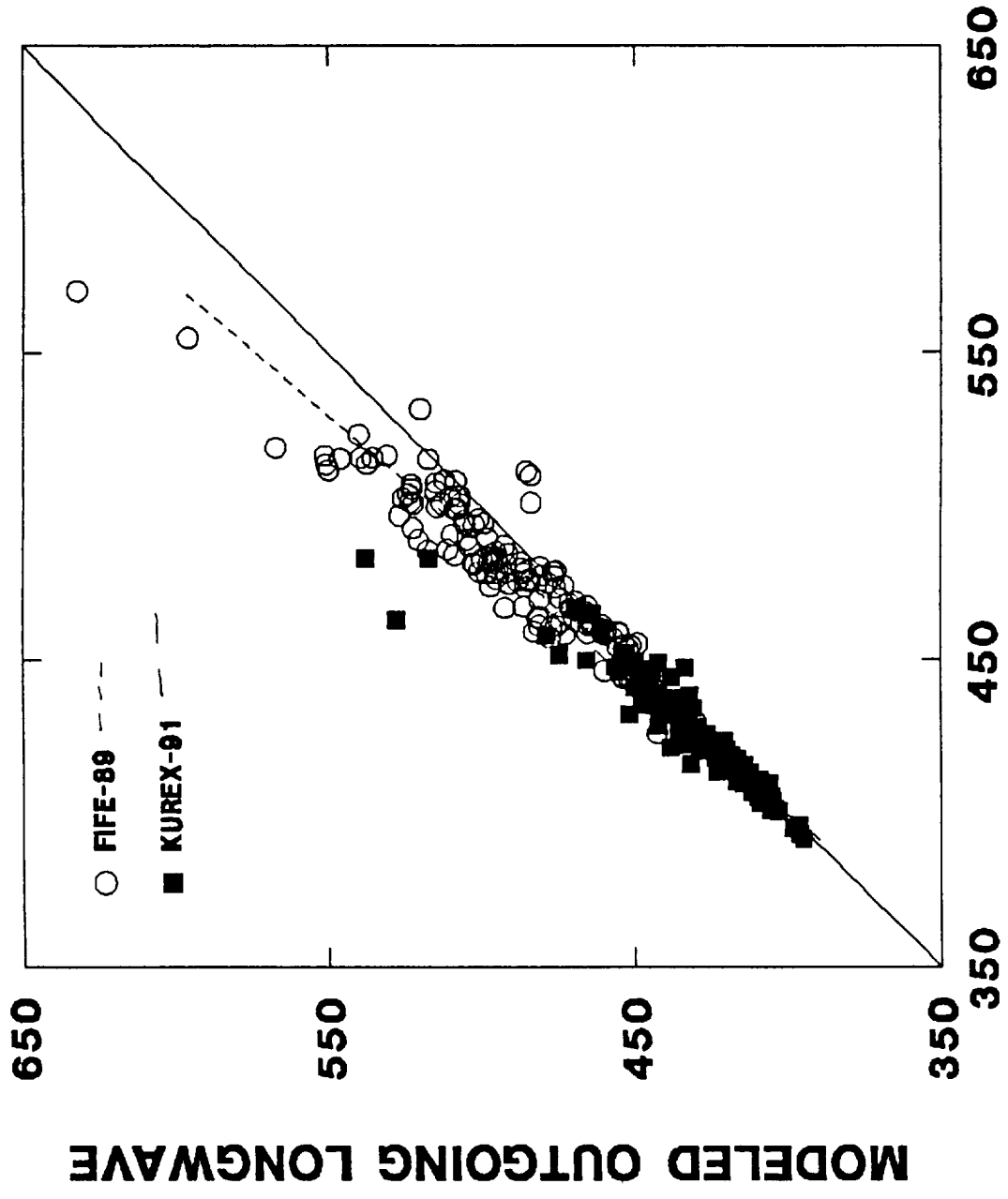


— Kurex Bound computed
 - - - Fife Bound computed
 avg. schedule data for plot
 Parameters - normal 4 sigma normal
 station

MEASURED INCOMING LONGWAVE

Figure 1 - Scatter Plot of (measured vs modeled)

Fig 1



MEASURED OUTGOING LONGWAVE

*FIFE - 89
KUREX - 91*

*FIFE - ± 35% model error
KUREX - ± 45% model error*

ORIGINAL PAGE IS
OF POOR QUALITY

Fig. 8

**ESTIMATING NET RADIATION WITH REMOTELY SENSED DATA:
RESULTS FROM KUREX-91 AND FIFE STUDIES¹**

B.L. Blad*, E.A. Walter-Shea, M.A. Mesarch and C.J. Hays
Department of Agricultural Meteorology
University of Nebraska, Lincoln, NE

P.J. Starks
USDA-ARS
National Agriculture Water Quality Laboratory
Durant, OK

D.W. Deering and T.F. Eck
NASA/Goddard Space Flight Center
Greenbelt, MD

ABSTRACT

Net radiation (R_n) is the major source of energy for evaporating water, heating the soil and air, and photosynthesis. The objective of this study is to estimate this important parameter with various models that have been developed to estimate the radiation balance components with remotely sensed data, and readily available meteorological data. Data used in this paper were collected over grassland vegetation during the FIFE-87, -88, -89 studies and the KUREX-91 study. For all studies estimated values of R_n were within about 10% of measured R_n . For the KUREX-91 study, measured and estimated R_n agreed to within about 1%. Improvement in a model(s) to estimate the reflected shortwave flux would provide an even better estimate of R_n since in all studies the reflected radiation stream was overestimated compared to the measured values. There was no clear trend for under or overestimation of incoming shortwave radiation from study to study. Components of the longwave balance were estimated with low mean relative errors when the incoming longwave flux was corrected for a bias in clear daytime values. Thus, it appears feasible to use remotely sensed data to estimate the incoming and outgoing shortwave radiation fluxes and the outgoing longwave radiation flux and to combine these fluxes with estimates of the incoming longwave radiation flux estimated from models which incorporate air temperature and vapor pressure data.

Keywords: net radiation, radiation balance, reflected radiation, albedo, remote sensing

* Address correspondence to Dr. B.L. Blad, Dept. of Agric. Meteorology, Univ. of Nebraska, Lincoln, NE 68583-0728

¹Published as Paper No. _____, J. Ser., Nebraska Agric. Res. Div.

Received _____ 1993, revised _____

INTRODUCTION

Net radiation (R_n) is the balance of the incoming (\downarrow) and outgoing (\uparrow) shortwave ($0.3 \mu\text{m}$ - $4.0 \mu\text{m}$) and longwave (4 - $100 \mu\text{m}$) radiation streams as shown in Eq. (1) where

$$R_n = R_{s\downarrow} - R_{s\uparrow} + R_{l\downarrow} - R_{l\uparrow}, \quad (1)$$

where R_s is the shortwave (solar) radiation and R_l is the longwave radiation. R_n is the fundamental quantity of energy available at the earth's surface to drive the processes of photosynthesis, evaporation of water, and heating of the soil and air (Rosenberg et al., 1983). It varies spatially and temporally. It can be measured at specific locations with net radiometers, but since it is strongly influenced by the surface over which it is measured, it is difficult to extend measurements made at a specific location to other sites, especially if the surfaces are heterogeneous. However, the shortwave and longwave incoming radiation components of net radiation are essentially independent of surface conditions so that ground point measurements of these components can be extrapolated to regional scales or can be estimated using radiative transfer models.

Remote sensing offers the potential to estimate reflected and emitted radiation from different types of surfaces and over areas of various sizes. Satellites and other remote sensing instruments measure only part of the total energy reflected from a surface whereas the total hemispherical reflectance or hemispherical emittance is required to compute the radiation balance (Eq. 1). Therefore, it is necessary to develop algorithms and techniques to estimate hemispherical reflectances and emittances using spectral data collected by remote sensors with restricted fields of view and over discrete wavebands. To extend discrete wavebands at limited viewing directions to cover the full spectrum hemispherically, the fractional contribution from each waveband must be multiplied by an appropriate weighting coefficient and summed to represent the total reflected radiation.

The incoming shortwave radiation component is typically measured with an upright pyranometer. Point measurements of incoming shortwave may be extended to a much larger area if atmospheric scattering and absorbing properties are assumed to be uniform over the region. Radiative transfer models are useful for estimating incoming conditions (e.g., the complex model of Dave *et al.*, 1975 and the simple model of Bird & Riordan, 1984). Others have evaluated use of satellite data to produce estimates of incoming shortwave at the spatial resolution of a given sensor (Hanson, 1971; Tarpley, 1979; Gautier *et al.*, 1980; Diak & Gautier, 1983). Starks, *et al.*, 1991 describes

an approach to estimate $R_s \downarrow$ from radiation reflected from a barium sulfate or molded, halon panel measured with a spectral radiometer.

A number of studies have been undertaken to estimate reflected shortwave radiation streams or surface albedo using data from instruments which measure spectral reflectance with restricted fields of view and then to compare these estimates with values measured with hemispherical pyranometers (Jackson, 1984; Irons *et al.*, 1988; Starks *et al.*, 1991). The Starks *et al.* method was employed in 1987 and 1988 at the FIFE site and yielded estimates of $R_s \uparrow$ with mean relative errors of about 20-25%.

The $R_l \downarrow$ term in Eq. 1 is typically measured with an upward-facing pyrgeometer. Numerous empirical and/or theoretical formulae to calculate incoming longwave radiation have been developed. Simple formulae for clear sky conditions were evaluated and are discussed in a companion paper (Starks *et al.*, this issue). The $R_l \uparrow$ term can be estimated from surface temperature measurements made with infrared thermometers or thermal scanners. A brief discussion of this approach is also given in the Starks *et al.* (this issue) paper.

Jackson *et al.*, (1985), Daughtry *et al.*, (1990), and Kustas & Daughtry (1990) have shown the potential of remote sensing to estimate net radiation using slightly different methods from those described in this paper. The primary objectives of this study are: (1) to test the validity of the procedure proposed by Starks *et al.* (1991) to estimate the shortwave radiation balance from grassland surfaces for the KUREX-91 and FIFE-89 studies using spectral bidirectional reflectances and (2) to combine these estimates of the shortwave radiation balance with estimates of the longwave radiation balance discussed in a companion paper (Starks *et al.*, this issue) to test the feasibility of estimating net radiation using remotely sensed data. Measurements made during FIFE-87, -88, -89 and KUREX-91 are used to evaluate the approach proposed by Starks (1990) to estimate R_n .

MATERIALS AND METHOD

Experiments were conducted on the Konza Prairie (Kansas, USA) during the FIFE-87, -88, -89 studies and on the Streletskaia Steppe Reserve (Russia) during the KUREX-91 experiment. Canopy shortwave spectral bidirectional reflectance, directional canopy temperature and the various components of the radiation balance (incoming and outgoing shortwave and longwave radiation streams) were measured. FIFE-89 data were obtained

for a burned, ungrazed grassland site. KUREX-91 data were taken at two grassland sites--a site mowed in 1989 but not in 1990 or 1991 (site 12), and one which had not been mowed for several years (site 14).

The FIFE-87 and -88 data were obtained from sites of varying vegetative condition. At the different sites, leaf area indices ranged from 0.3 to 3.0. Some sites were heavily grazed, others were not grazed or burned for many years. Sites were located on lowlands, hilltops and slopes of varying aspect and inclination.

Bidirectional reflectance data were obtained with a Barnes² Model 12-1000 Modular Multiband Radiometer (MMR) at the FIFE-87 through -89 sites and with the Goddard PARABOLA instrument (Deering & Leone, 1986) at the KUREX-91 sites.

The MMR measures reflected shortwave radiation in seven wavebands: 0.45-0.52 μm , 0.52-0.60 μm , 0.76-0.90 μm , 1.15-1.30 μm , 1.55-1.75 μm , and 2.08-2.35 μm ; and emitted radiation in the 10.5-12.5 μm waveband. The instrument was set with a 15° field of view and mounted on a portable mast that maintained a distance of 3.1 m from the soil surface. Measurements were made from seven view zenith angles in the solar principal plane: nadir and 20, 35 and 50° to either side of nadir. Incident radiation was estimated from MMR measurements made approximately every 30 min over a calibrated painted barium sulfate panel for FIFE-87 and over a calibrated 1.2 x 1.2 m molded, sintered polytetrafluorethylene-based (Spectralon) panel (Labsphere Inc.,² North Sutton, NH) during FIFE-88 and -89.

The PARABOLA was mounted on the end of a 6 m boom supported on a large tripod. The PARABOLA has a 15° field of view and measures radiation in the 0.650-0.670, 0.810-0.840 and 1.620-1.690 μm waveband region. The scanning head turns on two axes, which enables the acquisition of radiance data for almost the complete (4π) sphere. Irradiance is estimated from the nadir position over a calibrated painted barium sulfate reference panel. For this study, only the PARABOLA reflected data in the solar principal plane were used to simulate conditions under which the MMR collected data.

The method of Walthall *et al.* (1985) was used to simulate directional hemispherical reflectance from the solar principal plane reflected data. The SPECTRAL 2 model developed by Bird and Riordan (1984) was used to develop weighting coefficients to extend the spectral data collected by the MMR and PARABOLA to the entire solar

²Use of company or tradenames is for informational purposes only and does not imply endorsement by the University of Nebraska, the United States of Agriculture, or the National Aeronautics and Space Administration.

spectrum. The approach of Starks *et al.* (1991) was then used to combine the directional-hemispherical reflected radiance with weighting coefficients to produce estimates of surface albedo.

Each component of the radiation balance was measured using instruments mounted on an A-frame which was moved from site to site and/or from instruments mounted on the SERBS system at the KUREX-91 sites (Fritschen, this issue). At the KUREX-91 sites incoming and reflected shortwave components were obtained from Eppley Precision Spectral Radiometers² (PSP) in association with PARABOLA measurements (Deering and Eck, this issue). Incoming and outgoing longwave radiation streams were measured with Eppley Precision Infrared Radiometer PIR pyrgeometers². Net radiation was measured with REBS net radiometers mounted on the A-frame 1-1.5 m above the top of the vegetation. For the FIFE-89 studies all components of the radiation balance were measured from instruments mounted on a portable A-frame, or from automated mesonet stations located near the sites where remotely sensed data were collected. These instruments included an upright and inverted Eppley Precision Spectral Radiometer (model PSP), REBS net radiometer² (Q*3), and upright and inverted Eppley Pyrgeometers. The instruments on the A-frame were mounted to be approximately 1 m above the soil surface. The statistical methods used by Starks *et al.* (1991) were followed. The "d" index of model agreement they used was developed by Wilmott and Wicks (1980) and Wilmott (1981, 1982). Definitions of the statistical parameters are given in the footnote of Table 1.

RESULTS AND DISCUSSION

Estimation of $R_s\downarrow$, $R_s\uparrow$ and Albedo

The approach suggested by Starks *et al.* (1991) was used to estimate the incoming solar radiation flux density from nadir-viewed reflected reference panel data collected by the MMR and PARABOLA. Modeled values for FIFE-89 and KUREX-91 data are compared with measured values in Figure 1 and Table 1 ($d = 0.99$, $MRE = 6\%$; and $d = 0.99$, $MRE = 0.04\%$ for KUREX-91 and FIFE-89, respectively). The results show good agreement between the measured and modeled values, with a slight tendency for the model to overestimate the flux density of solar radiation, especially at flux densities below about 500 Wm^{-2} . This good agreement between measured and modeled values suggests that the approach used here is feasible for estimating $R_s\downarrow$.

The reflected shortwave radiation stream was estimated with the method given by Starks *et al.* (1991) using the MMR and PARABOLA solar principal plane data. Estimated values are compared with measured values in Figure 2 and Table 2. There was a definite trend for the modeled reflected shortwave fluxes to be greater than measured values with MRE values of 17.7 and 19.0%, and d indices of 0.92 and 0.69 for the KUREX-91 and FIFE-89 data, respectively.

Data shown in Figures 1 and 2 were used to calculate the albedo of the surface. Results are given in Figure 3 and Table 3. Modeled values tended to be higher than measured albedo by about 2% with a MRE of about 11% at KUREX-91 and by approximately 3% with a MRE of about 19% at FIFE-89. These findings are similar to those reported by Starks *et al.* (1991) for data collected during the FIFE-87 and -88 studies. Possible reasons for modeled albedos being higher than measured ones were suggested by Starks *et al.* (1991). These include: the use of weighting coefficients which are based upon incoming global solar radiation rather than spectral reflectance from vegetation, shadowing of the surface seen by the hemispherical instruments on the A-frame, and inadequate accounting for radiation coming from the hot spot in the Walthall *et al.* (1985) model for estimating bidirectional reflectance.

Coincident measurements of incoming and reflected shortwave components with the MMR and PARABOLA over the same surface characteristics at FIFE-87 and FIFE-89 (although limited, $N = 13$) provide an opportunity to evaluate any differences resulting from the use of the different radiometers (PARABOLA data were limited to solar principal plane to mimic the method used with the MMR). The same trends are indicated in both sets of data. The PARABOLA overestimated both incoming and outgoing shortwave radiation streams while the MMR underestimated the incoming solar radiation and overestimated outgoing shortwave radiation (Table 4). Note that the agreement of the reflected shortwave component for the PARABOLA and MMR estimates with measured values is not strong (with d statistics of 0.52 and 0.68, respectively).

Eck & Deering (this issue) investigated the effect of using spectral reflectance from vegetation to compute appropriate weighting coefficients. Using that approach, the PARABOLA estimates of albedo were slightly better than estimates derived from MMR data using weighting coefficients derived from incoming solar radiation.

Estimation of R_n

Net radiation estimates for FIFE-87 and FIFE-88 were made using R_s↓ and R_s↑ data presented in Starks *et al.* (1991) combined with R_l↓ estimates given in Starks *et al.* (this issue). The R_l↑ values were calculated using the Stefan-Boltzmann equation with T_r obtained using a nadir view. The results of the modeled R_n versus the measured REBS R_n are graphed in Fig. 4. The statistical data for these comparisons are given in Table 5. For these two years the *d* and *r*² values are all high, indicating close agreement between measured and modeled values and MRE values are less than 7%. In 1987 the estimated R_n was slightly lower than the REBS measured value, but in 1988 it was slightly higher. The close agreement of the estimated R_n with measured R_n during these two years is a little misleading because of compensating errors. The uncorrected error in the estimate of R_l↓ was larger than that for the corrected R_l↓ but was opposite in sign from the estimate of R_s↓. These errors tended to bring the total estimated incoming radiation stream closer to the measured value.

Net radiation was also calculated from measurements of each component radiation stream ("measured components" in Table 5) and compared to the REBS measured R_n. A small systematic error of less than about 10 W m⁻² is observed for these data. The *d* statistic indicates the agreement between the component estimated R_n and the REBS measured R_n is just slightly better than the agreement between the REBS measured R_n and estimated R_n.

For the FIFE-89 and the KUREX-91 studies, the estimated components of the shortwave radiation balance described earlier in this paper were combined with the longwave balance components discussed in the Starks *et al.* (this issue) companion paper. The net radiation was calculated using the bias adjustment in R_l↓ suggested by Starks *et al.* and also without this adjustment. R_n was also calculated from the measured individual component parts of the radiation balance. The statistics for comparing REBS measured R_n with estimated and measured component R_n are presented in Table 6, and REBS measured and estimated R_n values (adjusted R_l↓) are shown in Fig. 5. These data indicate a better agreement between REBS measured R_n and estimated R_n for the KUREX-91 study than with the FIFE-89 study. However, the agreement is more a result of cancelling errors than one of improved estimates. In the KUREX-91 study, the incoming and outgoing shortwave radiation streams were overestimated yielding a slight overestimate of the shortwave balance. The incoming longwave stream was underestimated while the outgoing longwave stream was overestimated yielding an underestimate of the longwave balance. The overall effect (i.e., from a slight overestimate of shortwave balance and an underestimate of the longwave balance) is for

the error in estimating the net radiation balance to be near zero ($MBE = -4 \text{ Wm}^{-2}$). At FIFE-89 the outgoing shortwave stream was overestimated while the incoming shortwave stream was only slightly underestimated yielding an underestimate of the shortwave balance. The incoming longwave stream was underestimated while the outgoing was overestimated yielding an negative longwave balance. The net effect was an underestimate of the net radiation balance ($MBE = -55 \text{ Wm}^{-2}$). The results for FIFE-87 were similar to those of FIFE-89 while the results for FIFE-88 were similar to KUREX-91. In all cases, R_n was estimated with MRE values of about 10% or less.

CONCLUSIONS

The results of this study suggest that R_n can be reliably estimated with remotely sensed data combined with some readily available meteorological data. In fact, R_n was estimated almost as well with remotely sensed inputs as when individual components of the radiation balance were measured and used to compute R_n . The agreement between measured and estimated R_n was particularly good when canopy cover was complete. Under near full-canopy cover, conditions measured and estimated values were generally within 5%. The agreement was especially good for the KUREX-91 study with MRE values of about 1%. The major flaw in the approach described in this paper is the overestimation of the reflected shortwave radiation flux density. A better approach for estimating this component of the radiation balance is needed. Improvements are likely to result from use of weighting coefficients developed from spectral radiation curves derived from radiation reflected from vegetation and from a model which adequately accounts for the reflected radiation from the hot spot.

ACKNOWLEDGEMENTS

This work was performed under NASA Contracts NAG5-894 and NAG5-1762. The authors wish to thank Roel Vining, Dave Klazinski, Doug Eschelbrenner, Pedro Zara, Gregory Grosshans, and Vicki Samson for their help in collecting the field data. Our thanks are extended to NCAR for providing the PAM data and S.B. Verma for the FIFE-89 Site 911 vapor pressure and air temperature data. We appreciate the efforts of Sharon Kelly, who typed the manuscript.

REFERENCES

- Bird, R. and Riordan, C. 1984. Simple solar spectral model for direct and diffuse irradiance on horizontal and tilted planes at the earth's surface for cloudless atmospheres. Solar Energy Research Institute, Golden, CO.
- Dave, J., Halpern, P. and Braslau, N. 1975. Spectral distribution of the direct and diffuse solar energy received at sea-level of a model atmosphere. Report G320-3332, IBM Palo Alto Scientific Center.
- Daughtry, C.S.T., Kustas, W.P., Maran, M.S., Pinter, Jr., P.J., Jackson, J.D., Brown, P.W., Nichols, W.D., and Gay, L.W. 1990. Spectral estimates of net radiation and soil heat flux. *Remote Sens. Environ.* 32:111-124.
- Deering, D.W. and Eck, T.F. 1993. Spectral bidirectional reflectance and angular distribution characteristics of Russian steppe vegetation and comparisons with continental U.S. prairie grasslands. *Remote Sens. Rev.* this issue.
- Deering, D.W. and Leone, P. 1986. A sphere-scanning radiometer for rapid directional measurements of sky and ground radiance. *Remote Sens. Environ.* 10:1-24.
- Diak, G. and Gautier, C. 1983. Improvements to a simple physical model to estimated incident solar radiation at the surface from GOES satellite data. *J. of Appl. Meteorol.* 22:505-508.
- Eck, T.F. and Deering, D.W. 1993. Spectral bidirectional hemispherical reflectance characteristics of selected sites in the Streletskaya Steppe. *Remote Sens. Rev.* this issue.
- Fritschen, L. 1993. Energy and radiation balance components for three grass surfaces near Kursk, Russia. *Remote Sens. Rev.* this issue.

- Gautier, G., Diak, G., and Masse, S. 1980. A simple physical model to estimate incident solar radiation at the surface from GOES satellite data. *J. Appl. Meteorol.* 19:1005-1012.
- Hanson, K. 1971. Studies of cloud and satellite parameterization of solar irradiation at the earth's surface. *Proc. of the Miami Workshop on Remote Sensing*, U.S. Dept. of Commerce, 133-148.
- Irons, J., Ranson, K., and Daughtry, C. 1988. Estimating Big Bluestem albedo from directional reflectance measurements. *Remote Sens. Environ.* 25:185-199.
- Jackson, R.D. 1984. Total reflected solar radiation calculated from multi-band sensor data. *Agric. For. Meteorol.* 33:163-175.
- Jackson, R.D., Pinter, P.J., and Reginato, R.J. 1985. Net radiation calculated from remote multispectral and ground station meteorological data. *Agric. For. Meteorol.* 35:153-164.
- Kustas, W.P. and Daughtry, C.S.T. 1990. Estimation of the soil heat flux/net radiation ratio from spectral data. *Agric. For. Meteorol.* 49:205-223.
- Mesarch, M.A., Walter-Shea, E.A., Blad, B.L., Hays, C.J., and Middleton, E.M. 1993. Comparing biophysical properties of the Streletskaya Steppe Reserve and the Konza Prairie. *Remote Sens. Rev.*, this issue.
- Rosenberg, N.J., Blad, B.L., and Verma, S.B. 1983. *Microclimate: The Biological Environment*. 2nd Edition. John Wiley and Sons, New York, 495 pp.
- Starks, P.J. 1990. *Measured and modeled radiation fluxes*. Ph.D. Dissertation, University of Nebraska, 179 pp.

- Starks, P.J., Norman, J.M., Blad, B.L., Walter-Shea, E.A., and Walthall, C.L. 1991. Estimation of shortwave hemispherical reflectance (albedo) from bidirectionally reflected radiance data. *Remote Sens. Environ.* **38**:123-134.
- Starks, P.J., Blad, B.L., Walter-Shea, E.A., Hays, C.J., and Mesarch, M.A. 1993. Estimation of the longwave radiation balance components: KUREX-91 and FIFE studies. *Remote Sens. Rev.*, this issue.
- Tarpley, J. 1979. Estimating incident solar radiation at the surface from geostationary satellite data. *J. Appl. Meteorol.* **18**:1172-1181.
- Walthall, C.L., Norman, J.M., Welles, J.M., Campbell, G., and Blad, B.L. 1985. Simple equation to approximate the bidirectional reflectance from vegetative canopies and bare soil surfaces. *Appl. Optics* **24**:383-387.
- Willmott, C.J. 1981. On the validation of models. *Phys. Geogr.* **2**:184-194.
- Willmott, C.J. 1982. Some comments on the evaluation of model performance. *Bull. Am. Meteorol. Soc.* **63**:1309-1313.
- Willmott, C.J. and Wicks, D.E. 1980. An empirical method for the spatial interpolation of monthly precipitation within California. *Phys. Geogr.* **1**:59-73.

Table 1. Statistics from comparison of incoming shortwave estimations with measured values using FIFE-89 MMR and KUREX-91 PARABOLA datasets. $N_{\text{FIFE89}} = 155$ and $N_{\text{KUREX91}} = 22$.

Algorithm	d	r	r ²	MBE Wm ⁻²	MRE %	RMSE Wm ⁻²	Eu Wm ⁻²	Es Wm ⁻²	\bar{x} Wm ⁻²	s Wm ⁻²	cv
KUREX-91	0.99	1.00	1.00	25.9	6.0	31.9	10.5	30.1	709.7	182.8	0.26
measured									648.2	205.0	0.32
FIFE-89	0.99	0.99	0.98	-3.8	0.1	26.0	21.1	15.2	707.7	158.1	0.23
measured									711.5	171.4	0.24

where

$d = 1 - [\Sigma(E-M)^2/\Sigma(|E-x| + |M-x|)^2]$
 E = estimated value
 M = measured value
 x = mean measured value
 $RMSE = \{[(N^{-1}\Sigma(P-M)^2) + [N^{-1}\Sigma(P-E)^2]]^{1/2}$
 $Es = (N^{-1}\Sigma(P-M)^2)^{1/2}$
 $Eu = (N^{-1}\Sigma(P-E)^2)^{1/2}$
 P = predicted value from linear regression of estimated and measured values
 $MBE = N^{-1}\Sigma(E-M)$
 $MRE = N^{-1}[\Sigma((E-M)/M)]/[100]$
 $\bar{x} = N^{-1}\Sigma E$ or $N^{-1}\Sigma M$
 $s = [(N-1)^{-1}\Sigma(E-x)^2]^{1/2}$ or $[(N-1)^{-1}\Sigma(M-x)^2]^{1/2}$
 $cv = s/\bar{x}$

Table 2. Statistics from comparison of reflected shortwave estimations with measured values using FIFE-89 MMR and KUREX-91 PARABOLA datasets. $N_{\text{FIFE89}} = 155$ and $N_{\text{KUREX91}} = 22$.

Algorithm	d	r	r^2	MBE Wm^{-2}	MRE %	RMSE Wm^{-2}	Eu Wm^{-2}	Es Wm^{-2}	\bar{x} Wm^{-2}	s Wm^{-2}	cv
KUREX-91	0.92	0.98	0.97	19.5	17.7	20.5	6.3	19.5	152.0	36.0	0.24
measured									123.8	36.0	0.29
FIFE-89	0.69	0.92	0.85	22.4	19.05	23.63	7.4	22.4	141.0	19.4	0.14
measured									118.5	16.3	0.14

Table 3. Statistics from comparison of albedo estimations with measured Eppley albedo values using FIFE-89 MMR and KUREX-91 PARABOLA datasets. $N_{\text{FIFE89}} = 155$ and $N_{\text{KUREX91}} = 22$.

Algorithm	d	r	r^2	MBE	MRE %	RMSE	Eu	Es	\bar{x}	s	cv
KUREX-91	0.78	0.93	0.86	0.022	11.085	0.025	0.010	0.023	0.218	0.026	0.119
measured									0.196	0.022	0.112
FIFE-89	0.70	0.90	0.81	0.032	19.13	0.034	0.012	0.032	0.204	0.027	0.132
measured									0.172	0.025	0.145

Table 4. Statistics from comparison of incoming and reflected shortwave estimations with measured components using MMR and PARABOLA data from FIFE-87 and FIFE-89.
 N = 14

Component	Method	d	r	r ²	MBE Wm ⁻²	MRE %	RMSE Wm ⁻²	Eu Wm ⁻²	Es Wm ⁻²	\bar{x} Wm ⁻²	std Wm ⁻²	cv
Incoming	PARA	0.963	0.997	0.994	61.0	9.0	62.5	12.6	61.2	782.3	162.7	0.208
	MMR	0.990	0.996	0.992	-21.4	-2.6	29.8	12.7	26.9	700.0	149.5	0.208
	Meas.									721.4	165.8	0.230
Reflected	PARA	0.521	0.951	0.904	35.2	26.5	35.9	6.1	35.4	168.4	20.4	0.121
	MMR	0.676	0.971	0.942	22.9	17.1	23.4	4.4	23.0	156.0	19.1	0.123
	Meas.									133.2	15.6	0.117
Albedo	PARA	0.719	0.961	0.924	0.030	16.1	0.031	0.006	0.030	0.220	0.024	0.109
	MMR	0.651	0.944	0.891	0.038	20.2	0.039	0.009	0.038	0.228	0.027	0.118
	Meas.									0.190	0.025	0.132

Table 5. Net radiation estimates for FIFE-87 and FIFE-88 using $R_s \downarrow$ and R_{st} estimates presented in Starks et al. (1991) and $R_{l \downarrow}$ estimates given in Starks et al. (this issue). Outgoing longwave radiation estimated from nadir-viewed MMR data.

Method	d	r	r ²	MBE Wm ⁻²	MRE %	RMSE Wm ⁻²	Eu Wm ⁻²	Es Wm ⁻²	\bar{x} Wm ⁻²	s Wm ⁻²	cv
FIFE-87											
Measured components (n = 67)	0.99	0.99	0.98	10.5	2.3	19.6	16.5	10.6	493.1	130.3	0.26
Estimated components (n = 187)	0.96	0.97	0.94	-33.5	-6.6	44.5	28.8	33.9	476.0	114.6	0.24
REBS measured (n = 187)									509.5	115.3	0.23
FIFE-88											
Measured components (n = 56)	0.99	0.98	0.96	-7.1	-1.2	21.9	20.7	7.2	594.8	98.6	0.17
Estimated components (n = 56)	0.98	0.97	0.94	5.6	1.3	24.9	21.6	12.5	607.5	88.1	0.15
REBS measured (n = 56)									601.9	96.5	0.16

Table 6. Statistics from comparison of Rn from estimated components (reflected shortwave-Walthall model, incoming longwave-Brunt model, outgoing longwave average of off-nadir IRT or +/- 35° MMR channel 8), measured components (incoming and reflected shortwave, incoming longwave, outgoing longwave data), measured by the REBS net radiometer using FIFE-89 (n=155) and KUREX-91 (n=12) datasets. (top is with adjustments from Table 4 (Starks et al., 1993) and bottom is without adjustments)

Method	d	r	r ²	MBE Wm ⁻²	MRE %	RMSE Wm ⁻²	Eu Wm ⁻²	Es Wm ⁻²	\bar{x} Wm ⁻²	s Wm ⁻²	cv
KUREX-91 Measured components	0.98	0.97	0.95	4.6	0.6	23.5	19.8	12.6	508.3	91.7	0.18
Estimated components	0.99 0.98	0.99 0.99	0.98 0.98	-7.0 18.0	-1.3 3.8	12.8 20.8	9.7 9.7	8.4 18.4	496.7 521.7	73.3 73.3	0.14 0.14
REBS measured									503.7	77.1	0.15
FIFE-89 Measured components	0.99	0.99	0.98	0.3	-0.2	23.1	22.5	4.9	478.0	143.8	0.30
Estimated components	0.94 0.97	0.97 0.97	0.95 0.95	-54.6 -29.6	-11.3 -5.5	63.7 44.2	29.2 29.2	56.6 33.1	423.1 448.1	125.6 125.6	0.28 0.28
REBS measured									477.7	137.1	0.29

LIST OF FIGURES

- Fig. 1. Flux densities of incoming solar radiation estimated with the model of Starks *et al.*, (1991) compared with measured values at FIFE-89 and KUREX-91. The solid line is the 1:1 line.
- Fig. 2. Flux densities of reflected solar radiation estimated with the model of Starks *et al.*, (1991) compared with measured values at FIFE-89 and KUREX-91. The solid line is the 1:1 line.
- Fig. 3. Albedo values calculated from incoming and reflected solar flux densities obtained with the Starks *et al.*, (1991) model compared with measured values. The solid line is the 1:1 line.
- Fig. 4. Flux densities of net radiation from the radiation balance components in Figures 1, 2, 4 and 5, compared with R_n measured with the REBS net radiometer on the A-frame. The solid line is the 1:1 line.
- Fig. 5. Flux densities of net radiation from the radiation balance components for the FIFE-89 and KUREX-91 studies, compared with R_n measured with the REBS net radiometer on the A-frame. The solid line is the 1:1 line.

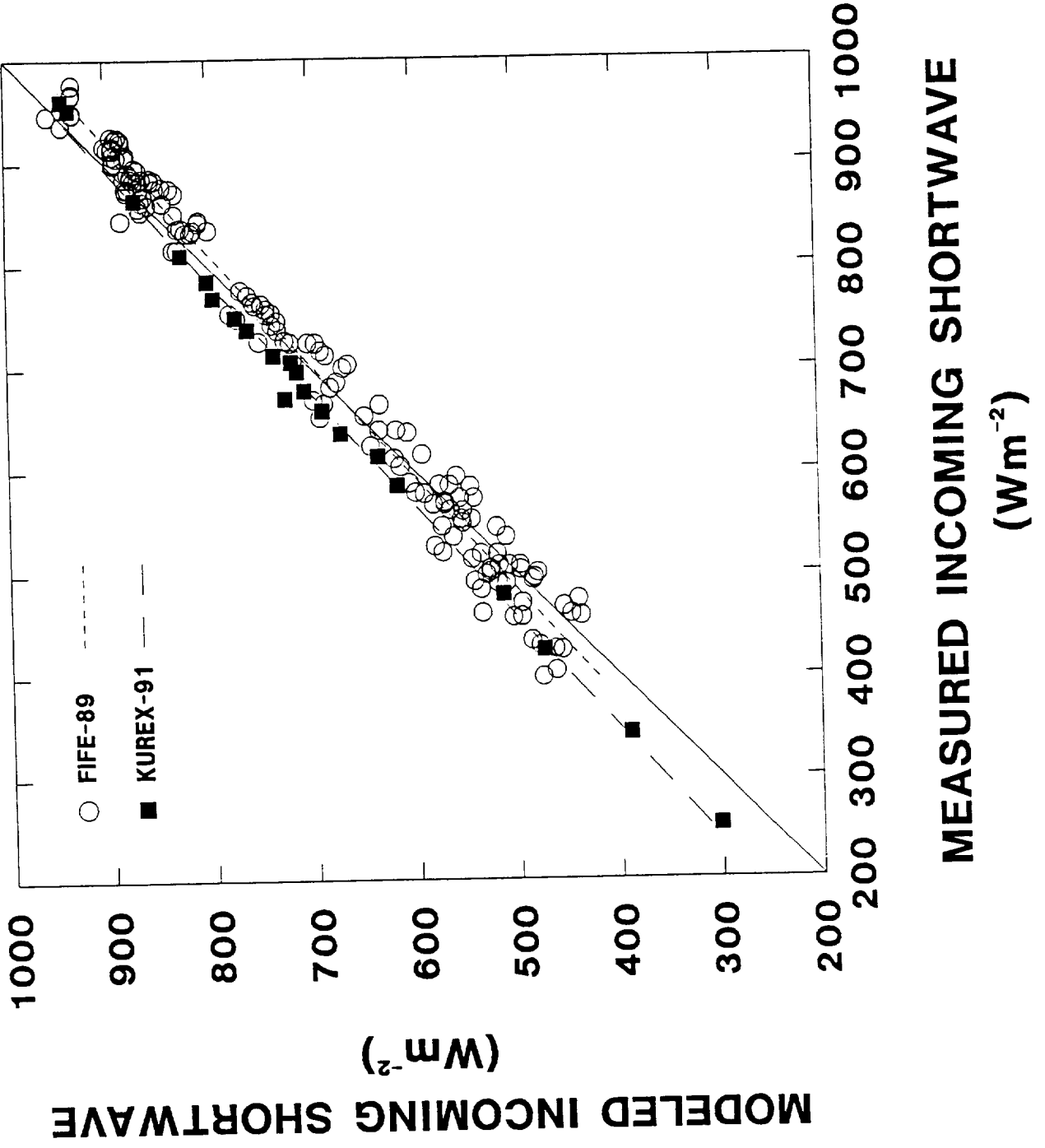
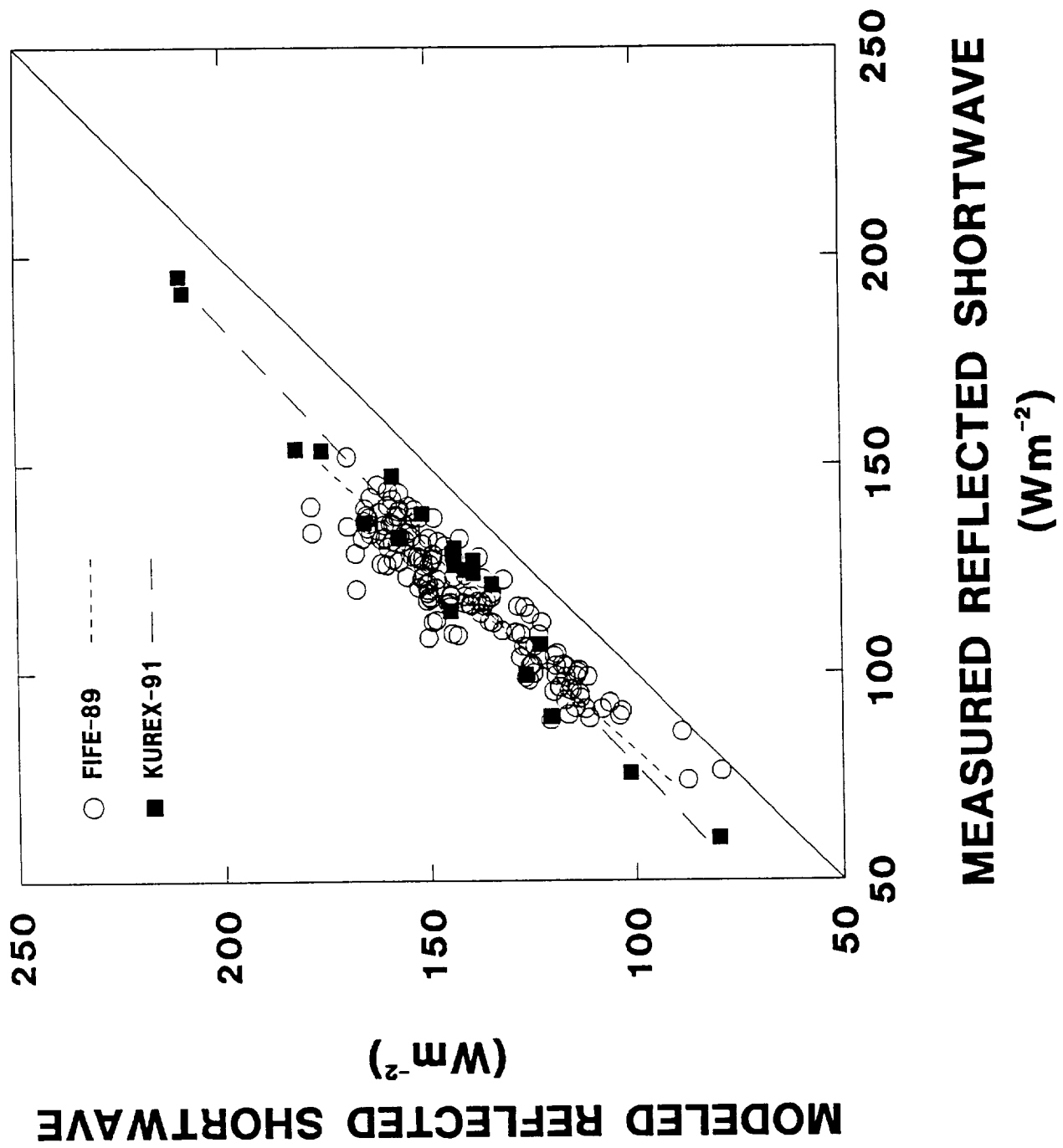
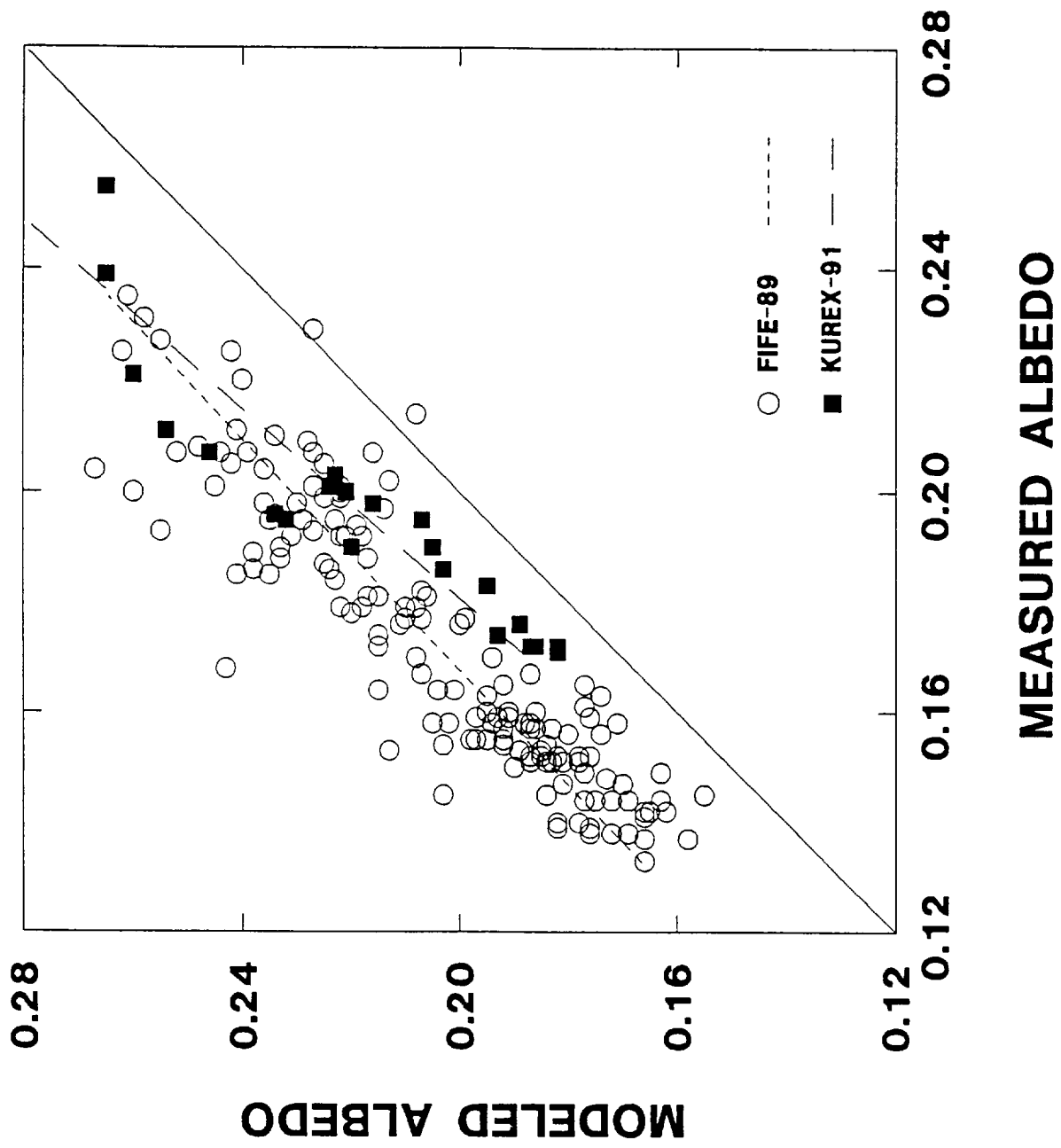
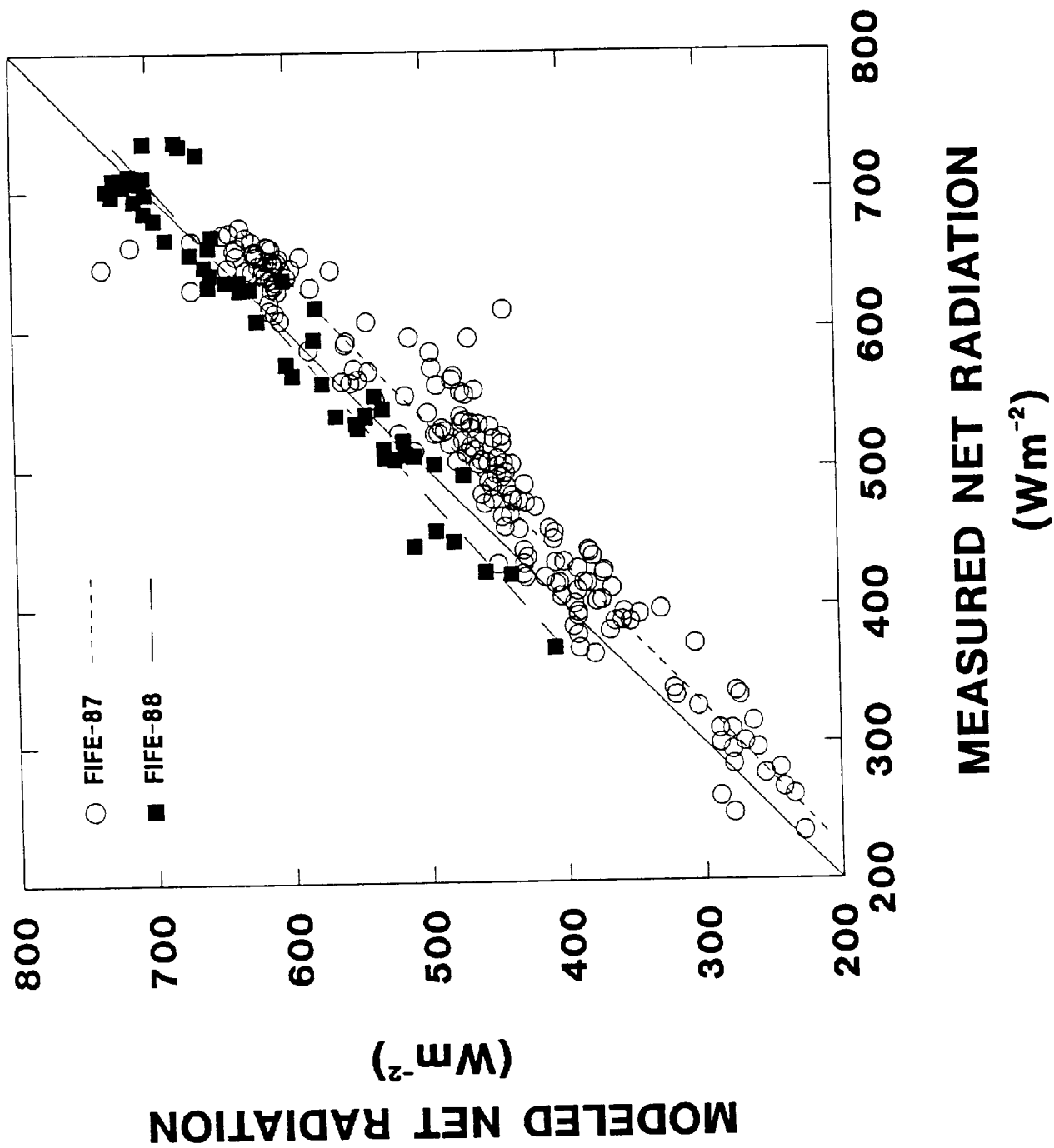


Fig 1







10/1

